EPJ Appl. Metamat. 2016, **3**, 3

DOI: 10.1051/epjam/2016005

EPJ Applied Metamaterials

Available online at:
http://epjam.edp-open.org

RESEARCH ARTICLE OPEN ACCESS

# Manipulating scattering features by metamaterials

Cui Lu[1], Zhong Lei Mei[1,*], Wen Xuan Tang[2,3], and Tie Jun Cui[2,3,*]

[1] School of Information Science and Engineering, Lanzhou University, Lanzhou 730000, P.R. China
[2] School of Information Science and Engineering, Southeast University, Nanjing 210096, P.R. China
[3] State Key Laboratory of Millimetre Waves, Southeast University, Nanjing 210096, P.R. China

Received 31 March 2016 / Accepted 30 May 2016

**Abstract –** We present a review on manipulations of electromagnetic scattering features by using metamaterials or metasurfaces. Several approaches in controlling the scattered fields of objects are presented, including invisibility cloaks and radar illusions based on transformation optics, carpet cloak using gradient metamaterials, dc cloaks, mantle cloaks based on scattering cancellation, "skin" cloaks using phase compensation, scattering controls with coding/programmable metasurfaces, and scattering reductions by multilayered structures. Finally, the future development of metamaterials on scattering manipulation is predicted.

**Key words:** matematerials, scattering manipulation, cloak, illusion device, transformation optics.

## 1 Introduction

Metamaterial is a kind of artificially structured material with exotic properties which are not found in nature. The effective medium property of metamaterial is not only relevant to the constitute material, but also decided by the microscopic structures. As a result, the electromagnetic (EM) responses of metamaterial can be tailored by tuning different unit geometries. The special physical properties and flexible controllability on EM waves of metamaterials have gained extensive attentions in the scientific field during the last 15 years. The left-handed material – a specific version of metamaterial, and EM invisibility cloak based on metamaterial have been listed as one of the breakthroughs of the year by the Science magazine in 2003 and 2006, respectively.

In the early years, metamaterial was referred to left-handed material with negative refractive index, whose name is due to the left-hand relationship between electric field, magnetic field and the wave vector when an EM wave propagates in the material. It was also named as backward wave material, and double negative material, etc. Left-handed material was firstly proposed by Veselago, a Soviet Union scientist, in 1968 [1], who predicted the fantastic and unusual EM properties such as the negative refraction (was later experimentally confirmed in 2001 [2]), reversed Cherenkov radiation (with experimental verifications in 2009 [3, 4]), and the reversed Doppler effect. Subsequent studies indicate that left-handed materials also have other bizarre properties, including reversed Goos-Hanchen shift [5], evanescent wave amplification [6], perfect lens effect [7], etc.

With the rapid developments of metamaterial technologies, the term "metamaterial" has gone far beyond left-handed or negative refractive index materials. At present, it has been widely accepted that metamaterials may contain all artificial composite materials with periodic/aperiodic structures and have fantastic EM properties, including gradient refractive index material [8], zero-index material [9–11], the left/right handed composite transmission line material [12], EM-parameter-tunable materials [13], etc. From this point of view, metamaterials, in a broad sense, also cover the well-developed artificial structures, such as photonic crystals [14], EM band-gap materials [15], and frequency selective surfaces [16].

In recent years, applications of metamaterials have attracted enormous interests due to their unusual properties. Metamaterials have been extensively applied in various EM devices or systems, including the invisibility cloaks [17–21], high-performance antennas [22–24], various lens structures [25–28], fabulous illusion devices [29–31], photonic devices [32, 33], and many other microwave and terahertz devices and systems [34–36]. In this review, however, we mainly focus our attention on the application of metamaterials in manipulating the scattering features of objects.

## 2 What is scattering manipulation?

When EM waves impinge on an object, e.g. an aircraft in the sky, the constitute materials of the object will be polarized

*e-mail: meizl@lzu.edu.cn; tjcui@seu.edu.cn

by the incident field, giving rise to enormous number of oscillating dipoles inside the object, which act as the secondary sources and re-radiate in the space. Macroscopically speaking, the incident waves are scattered by the object and redistributed in all directions. Quite naturally, these scattered fields depend on the geometry of the object, the shape, size, roughness of surface, and the constitutive materials inside the object. In other words, they carry the information of the object. Through analyzing the scattered fields, it is possible to identify the object in a distance. This fact lays the foundation of the modern radar technology, which is schematically illustrated in Figure 1a.

Different objects have different scattering features, just like the "fingerprint" of human beings. Then, is it possible to change this "fingerprint" and disguise the object as nothing or another one? This is exactly what scattering manipulation will do. Traditionally, people use weird shapes and irregular surfaces to reflect incident waves into other directions and hence reduce the possibility of detection, and this design has been adopted in various fighter planes. Another method is to paint the object with a coating layer, which can absorb the EM energy and make the object undetectable. However, we will not focus on these traditional methods in the current work.

With the development of metamaterial technology, novel approaches have been proposed to control the scattering features of an object. Among them, the transformation optics (TO) based invisibility cloak design is well known in the community. For this approach, a metamaterial-based shell is used to wrap the object, guide the incident EM wave around the object, and return to their original propagation as if nothing happens. Based on this idea, illusion shells can also be designed and implemented, which can change the "fingerprint" of one object into that of a pre-designed one. Moreover, one can even reverse the cloak design and extensively magnify the scattering of a certain object, and this is called the super-scattering scheme [37]. A schematic illustration of scattering manipulation is given in Figure 1b.

In most cases, the TO based shells are bulky, narrow-banded, and are difficult for practical realizations. To address the problem, a two-dimensional (2D) metamaterial with a very small thickness, termed as the metasurface, has been proposed. The metasurface consists of large number of resonant units, and can be used to enclose an object and change the scattering properties by geometrically tuning the unit cells. A skin cloak, which is used to cover an object and keep it from the overhead detection, has also been realized using the metasurface. In addition to the above methods, one can use a multilayered structure to wrap the object and modify the scattering feature by tuning the layer geometry, material parameters, and so on. In many cases, this scheme gives the most affordable and effective solution for the scattering manipulation.

In the following sections, we will discuss various scattering manipulation schemes, including the invisibility cloak [38], radar illusion [39], carpet cloak [40, 41], DC cloak [17], mantle cloak [42], an ultra-thin carpet cloak [43], digital and programmable metasurface [44], and multilayer structure based on optimizations [45–47]. Finally, we give the conclusion on this topic.

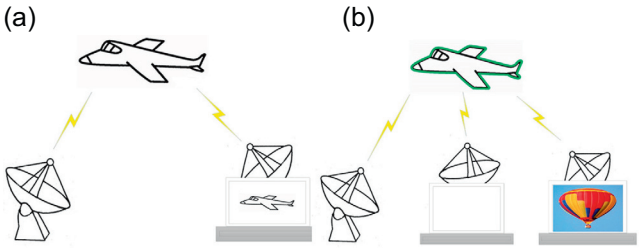


**Figure 1.** Object identification using a radar (a) and scattering manipulation to deceive it (b).

## 3 Perfect cloak based on transformation optics

With the in-depth researches on metamaterials, the corresponding novel devices have gained wide concerns. However, for a long time, there has not been a systematic method to support the design of these devices until a perfect EM cloak is ingeniously designed by Pendry et al. in 2006 [38]. This is a very beautiful thought. The fundamental theory behind the design, transformation optics, seamlessly bridges the gap between the metamaterial technology and novel EM devices.

Figure 2 shows the ray-tracing performance of the perfect cloak proposed by Pendry and coworkers. When the cloak is illuminated, the incident rays will be guided along the cloak, and no EM radiations can get into the concealed volume. However, after passing through the invisibility cloak, light rays restore to the original path again, as if they are propagating in the free space. Hence, an object with arbitrary shape can be hidden in the concealed space.

In realization of the perfect cloak, the EM parameters can be acquired by the TO theory. The fundamental of TO is the invariance of Maxwell's equations, which has exactly the same form in any coordinate system. However, the permittivity and permeability should be transformed in a unified manner. In the new coordinate system, the renormalized values of permittivity and permeability can be expressed as:

$$\varepsilon' = \frac{A\varepsilon A^T}{\det(A)}, \quad \mu' = \frac{A\mu A^T}{\det(A)}, \tag{1}$$

in which $(\varepsilon, \mu)$ and $(\varepsilon', \mu')$ are the constitutive tensors in the real space and the cloak space, respectively, and $A$ is the Jacobian matrix with components $A_{ij} = \partial x_i / \partial x_j$. It can be clearly seen that inhomogeneous and anisotropic materials are needed for the design, which can be nicely provided by the emerging metamaterials.

For Pendry's cloak, the 2D cylindrical design requires the following parameters:

$$\begin{aligned} \varepsilon'_r = \mu'_r = \frac{r - R_1}{r}, \varepsilon'_\theta = \mu'_\theta = \frac{r}{r - R_1}, \varepsilon'_z = \mu'_z \\ = \left(\frac{R_2}{R_2 - R_1}\right)^2 \frac{r - R_1}{r}. \end{aligned} \tag{2}$$

In order to facilitate the implementation, the transverse-electric (TE) polarization is further considered. The above materials can be approximately reduced into the following

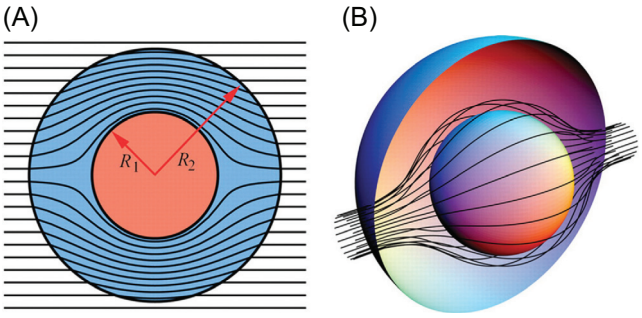


**Figure 2.** Ray-tracing performance of the invisibility cloak. (A) A 2D cross section of rays striking the system, diverted within the annulus of cloaking material contained within $R_1 < r < R_2$ to emerge on the far side undeviated from their original course. (B) A 3D view of the same process. From reference [38]. Reprinted with permission from AAAS.

form, in which only $\varepsilon'_r$, $\mu'_r$, and $\mu'_\theta$ are relevant, bearing in mind that both materials have the same performance in the sense of geometrical optics approximation [48]:

$$\varepsilon'_z = \left(\frac{R_2}{R_2 - R_1}\right)^2, \mu'_r = \left(\frac{r - R_1}{r}\right), \mu'_\theta = 1. \qquad (3)$$

The experimental verification for the first invisibility cloak was carried out by Smith's group in 2006 [48]. Figure 3 is the fabricated 2D microwave cloaking device with split-ring resonator (SRR) structured metamaterials.

Figures 4A and 4B are the simulations of the cloak with the exact and reduced material parameters, respectively, while Figures 4C and 4D are the experimental measurements of the bare conducting cylinder and the cloaked conducting cylinder, respectively. The comparison between Figures 4B and 4D indicates that the full-wave simulations with reduced materials are in good agreement with the experimental data. Though the invisibility is imperfect due to the approximations used and material absorption, this result does provide an experimental display of the EM cloaking mechanism. In addition to this, the theoretical frame of TO and the realization with metamaterials also establish a solid foundation for the design and implementation of other novel EM devices.

## 4 A radar illusion device using metamaterials

Under the radar detection, the scattering properties of different objects will differ significantly. However, if regulated appropriately, the scattering pattern of an object can be changed. For example, when wrapped with a properly designed metamaterial shell, the scattering pattern of one object can appear exactly the same as that of another one. As a result, the radar equipment will be confused and deceived, which is known as "illusion". The illusion device was first conceptually proposed by Lai et al. [29], capable of changing one object into another. Based on this theory, researchers have studied deeply on various illusion devices [49–52]. Jiang et al. proposed an

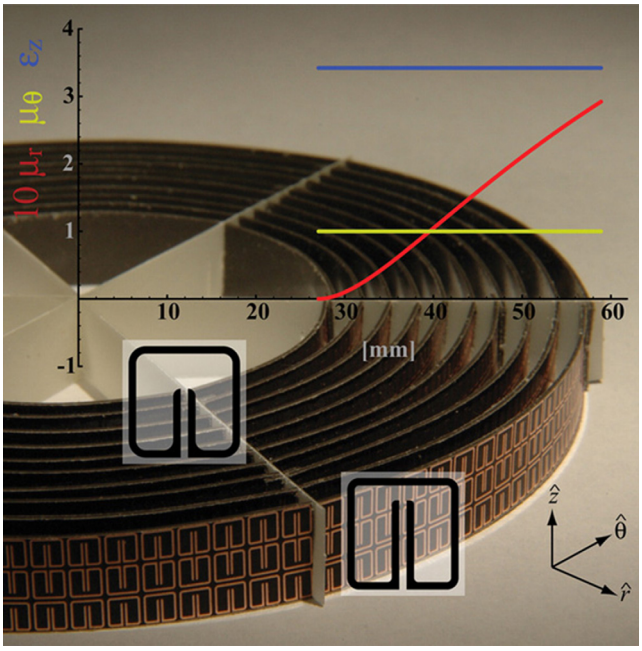


**Figure 3.** The 2D microwave cloaking structure (background image) with a plot of the material parameters that are implemented. $\mu'_r$ (red line) is multiplied by a factor of 10 for clarity. $\mu'_\theta$ (green line) has the constant value 1. $\varepsilon'_z$ (blue line) has the constant value 3.423. The SRRs of cylinder 1 (inner) and cylinder 10 (outer) are shown in expanded schematic form (transparent square insets). From reference [48]. Reprinted with permission from AAAS.

illusion device that can transform an arbitrary object virtually into a small-sized one with the desired parameters [53]. A virtual-shifting illusion device [54] was also proposed by the same group, which can render an arbitrary object located at one place to appear at another place.

Recently, based on TO theory and metamaterial technology, a ghost illusion device is proposed and designed by Jiang and coworkers [39], which can virtually transform the scattering signature of an arbitrary object into that of multiple arbitrarily-designed and isolated ghost objects. Figure 5 illustrates the functions of the ghost illusion device, where a perfectly conducting metallic object (Figure 5a) is transformed into three objects (Figure 5b). The corresponding radar signature of the covered metallic object (Figure 5b) is demonstrated in Figure 5e, which is accordance with the radar signature (Figure 5f) of a metallic object and two dielectric wings in Figure 5c. As a result, probing radar will wrongly identify the metal object as three separate objects.

Similar to the invisibility cloak, the ghost illusion device can be readily realized by TO and metamaterials. In this case, a cylindrical object (with radius $a$) and a ghost device (with outer radius $c$) are chosen in the physical space. While in the virtual space, there are three distinct objects: a shrunken object and two wing-ghosts, as shown in Figure 5c. For simplicity, two wing-ghosts are designed as an example. The radius of shrunken object is $a'$ and the inner and outer radii of wing-ghosts are $b'$ and $c$ respectively. One possible mapping for

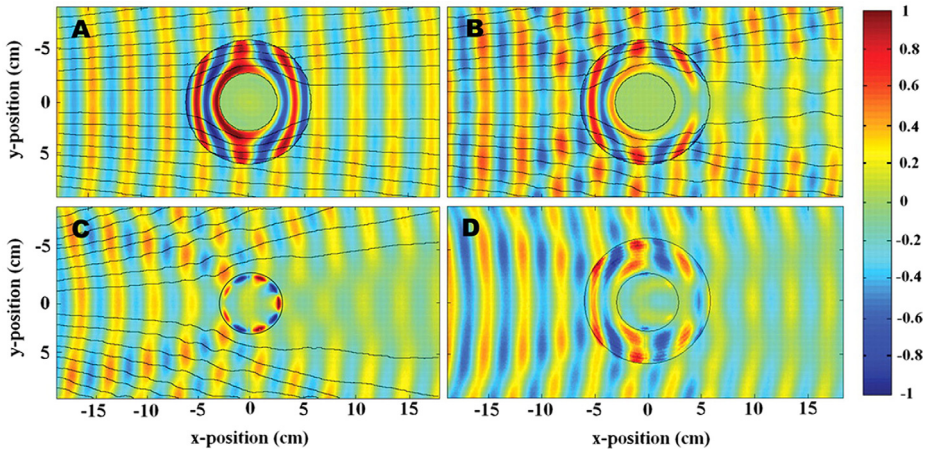


**Figure 4.** Snapshots of electric field patterns, with stream lines [black lines in (A–C)] indicating the direction of power flow. The cloak lies in the annular region between the black circles and surrounds a conducting Cu cylinder at the inner radius. The fields shown are (A) the simulation of the cloak with the exact material properties, (B) the simulation of the cloak with the reduced material properties, (C) the experimental measurement of the bare conducting cylinder, and (D) the experimental measurement of the cloaked conducting cylinder. From reference [48]. Reprinted with permission from AAAS.

the above ghost illusion device in general 3D case is given by [39]:

$$(r, \theta, \varphi) = (k(r' - a') + a, \theta', \varphi'), \tag{4}$$

where $k = \frac{c-a}{c-a'}$. Based on TO theory, the relative permittivity and permeability in region $a < r < c$ (except for the two wing-ghost areas) and the two wing-ghost areas can be described respectively by

$$(\varepsilon_r, \varepsilon_\theta, \varepsilon_\varphi) = (\mu_r, \mu_\theta, \mu_\varphi) = \left(\frac{1}{k}\left(\frac{r - a + ka'}{r}\right), \frac{1}{k}, \frac{1}{k}\right), \tag{5}$$

$$\begin{aligned}(\varepsilon_r, \varepsilon_\theta, \varepsilon_\varphi) &= (\mu_r, \mu_\theta, \mu_\varphi) \\ &= \left(\frac{1}{k}\left(\frac{r - a + ka'}{r}\right), \frac{1}{k}, \frac{\varepsilon_{\text{virtual}}}{k}\right),\end{aligned} \tag{6}$$

where $\varepsilon_{\text{virtual}}$ is the pre-designed permittivity of the ghost-wing targets. As we can see, these parameters are inhomogeneous and anisotropic, which are difficult to realize by the current metamaterial techniques. In order to be realized by artificial materials, the materials under TE polarization can be simplified as follows:

$$(\mu_r, \mu_\varphi, \varepsilon_z) = \left(\left(\frac{r - a + ka'}{r}\right)^2, 1, \frac{1}{k^2}\right), \tag{7}$$

$$(\mu_r, \mu_\theta, \varepsilon_z) = \left(\left(\frac{r - a + ka'}{r}\right)^2, 1, \frac{\varepsilon_{\text{virtual}}}{k^2}\right). \tag{8}$$

Then, in both parts of the ghost illusion device, $\mu_\varphi$ and $\varepsilon_z$ are constants, while only $\mu_r$ varies in the radial direction, which can be easily realized by artificial structured materials, such as SRR-based ones [48].

Figure 6 shows the designed ghost illusion device, which consists of eight concentric layers of low-loss printed circuit boards (PCBs) with each layer carrying three rows of SRRs. In region I, the permittivity maintains 2.82 and the permeability ranges from 0.065 to 0.226, while in region II, the permittivity maintains 6.29 and the permeability ranges from 0.226 to 0.355, which can be easily achieved by carefully tuning the size of SRRs.

Figure 7a illustrates the experimental setup together with the resultant 2D fields in the near zone. Figures 7b and 7d show the measurement and simulation results of the ghost device, respectively, which is accordance with each other. For more details, the simulated and measured electric field intensity along a pre-selected line can be seen in Figure 7c. In comparison, the harmony is observed between the two lines, proving the correctness of the design again.

## 5 Carpet cloak using gradient metamaterials

As we have shown in the previous sectors, cloaks based on transformation optics have been a very hot topic in recent years. However, most of the designed cloaks require inhomogeneous and anisotropic materials, and even singular parameters. Usually, they are realized with metamaterials using resonant unit cells, and thus have a narrow frequency band and relatively large loss. Though reduced cloaks have been demonstrated [48], these devices are realized at the cost of unsatisfied cloaking performance. Owing to the stringent requirement for the metamaterials, the realization of full cloak is still a challenge. To address these problems, carpet cloaks are proposed [40, 41, 55, 56]. These devices can cover an object on a ground plane and make it invisible from the above radar detection. The designed carpet cloaks have the advantages such as relatively simple EM parameters, easy realization, low loss, omni-direction, and so on.

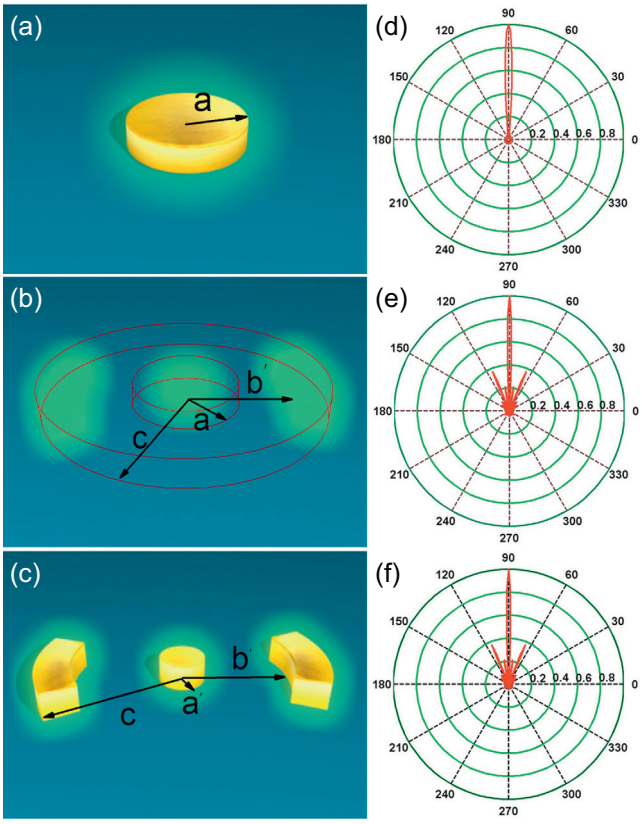


**Figure 5.** Schematic, composition, and equivalence of the ghost-illusion device. (a) The original metallic object with its scattering signature given in panel (d). (b) The metallic object covered by the designed ghost device and the corresponding scattering signature in panel (e). (c) A shrunk metallic object at the original center with two wing dielectric objects, whose signature is given in panel (f). The scattering signatures of (b, c) are completely the same. In the far-field calculation, the geometrical parameters are chosen as $a = 3.8\lambda_0$, $a' = 1.63\lambda_0$, $b' = 5.4\lambda_0$ and $c = 7\lambda_0$. Reprinted (figure) with permission from reference [39]. Copyright © 2013 WILEY-VCH Verlag GmbH & Co. KGaA, Weinheim.

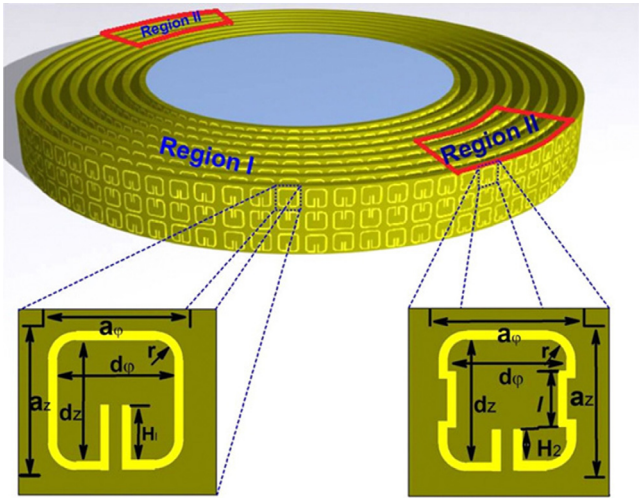


**Figure 6.** The conventional and modified SRRs constitute the ghost device following the parameters described in equations (7) and (8). Reprinted (figure) with permission from reference [39]. Copyright © 2013 WILEY-VCH Verlag GmbH & Co. KGaA, Weinheim.

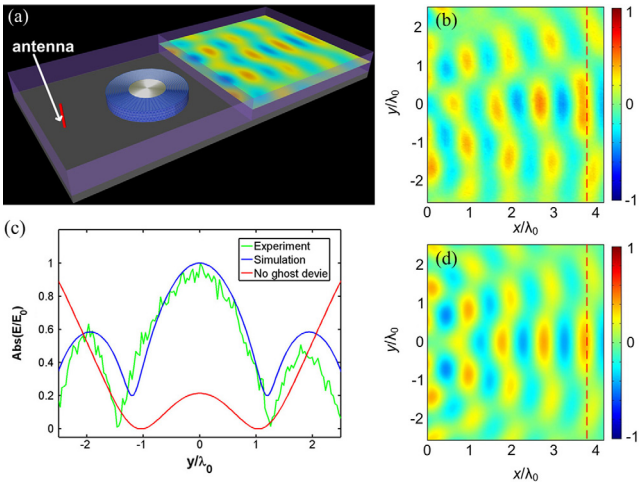


**Figure 7.** The experimental setup, simulation and experimental results of the ghost-illusion device. (a) Illustration of the experimental setup. (b) The measurement result. (c) The normalized intensity along the red dashed line $x = 3.8\lambda_0$. (d) The simulation result. Reprinted (figure) with permission from reference [39]. Copyright © 2013 WILEY-VCH Verlag GmbH & Co. KGaA, Weinheim.

The key ingredient for the carpet cloak design is the transformation function utilized in the TO frame. For general TO designs, arbitrary transformation functions are chosen, connecting the virtual and physical spaces. However, this arbitrariness also leads to the anisotropy of the resulted materials. Then, it is quite natural that an optimized transformation function can lead to a better design. Based on this idea, Pendry and Li proposed to use quasi-conformal mapping for the cloak, which can minimize the anisotropy of the resulted material and give rise to an approximated dielectric [55]. One obvious weak point does exist, this design can only be applied to "carpet" designs instead of fully-spatial cloaks.

It really works! Shortly after proposal of the carpet design, an experimental realization of a two-dimensional carpet cloak was delivered by Liu and coworkers [40]. In this design, the refractive index of the carpet was implemented with nonresonant metamaterial elements, i.e., the I-shaped unit cells, which not only can meet the required constitutive parameters but also have relatively wide bandwidth and low loss. The geometry of the constructed elements is determined by an automated design process. Figure 8 shows the fabricated carpet cloak, the unit cell, and the retrieved refractive index at different geometries.

Figure 9 demonstrates the measured electric field distribution at different operating frequencies. Figures 9A–9C represent the measured results for the ground, perturbation, and ground-plane cloaked perturbation, respectively, all at 14 GHz. Comparing the three results, one can see that Figures 9A and 9C agree well with each other. By covering the space surrounding the perturbation with a carpet cloak, the reflected

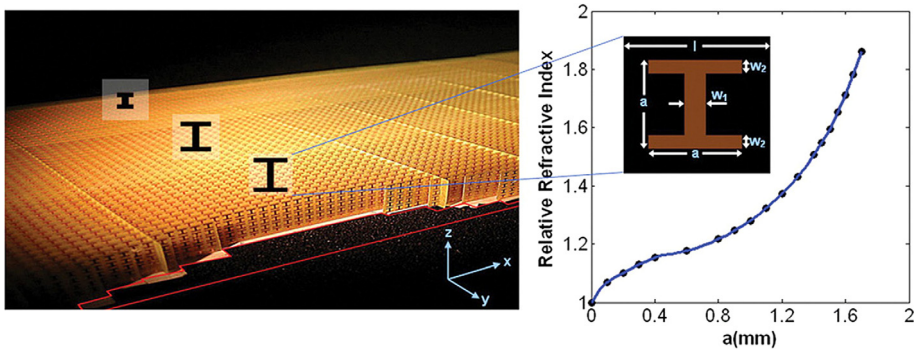


**Figure 8.** Photograph of the fabricated carpet cloak and the relation between the unit cell geometry and the effective index. The dimensions of the metamaterial unit cells are $l$ = 2 mm, $w_1$ = 0.3 mm, $w_2$ = 0.2 mm, and $a$ varying from 0 to 1.7 mm. From reference [40]. Reprinted with permission from AAAS.

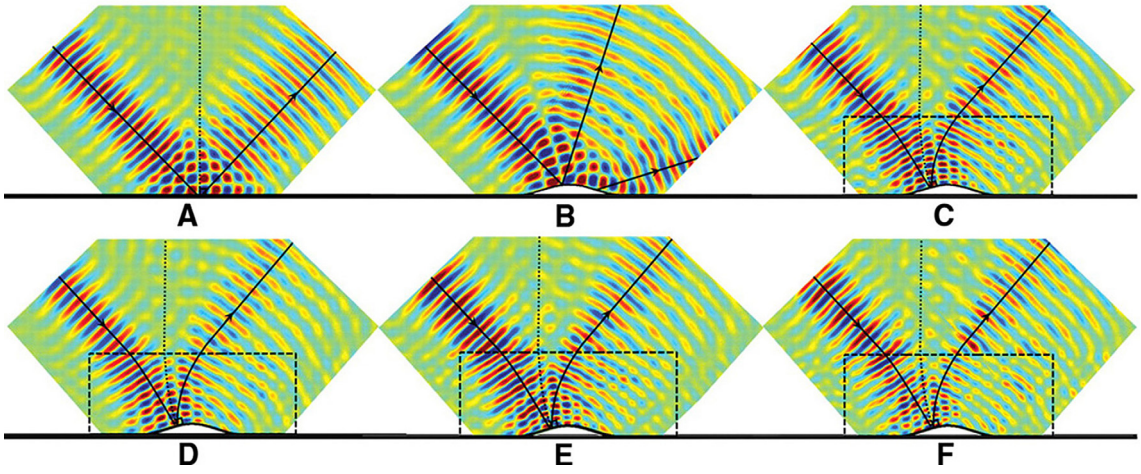


**Figure 9.** Measured field mapping (E-field) of the ground, perturbation, and ground-plane cloaked perturbation. The rays display the wave propagation direction, and the dashed line indicates the normal of the ground in the case of free space and that of the ground-plane cloak in the case of the transformed space. (A) Collimated beam incident on the ground plane at 14 GHz. (B) Collimated beam incident on the perturbation at 14 GHz (control). (C) Collimated beam incident on the groundplane cloaked perturbation at 14 GHz. (D) Similar to (C) but at 13 GHz. (E) Similar to (C) but at 15 GHz. (F) Similar to (C) but at 16 GHz. From reference [40]. Reprinted with permission from AAAS.

beam is restored as if the ground plane were flat. Besides, the wide-band characteristics of the cloak is tested at 13 GHz, 15 GHz, and 16 GHz, as shown in Figures 9D–9F respectively.

In 2010, our group designed and verified a 3D ground-plane cloak at the microwave frequencies [41]. This ground-plane cloak can conceal a 3D object located under a cone-shaped conducting plane from all viewing angles, the reflection of which is consistent with a flat conducting plane. Figure 10 demonstrates the designed 3D microwave ground-plane cloak and its refractive index distribution. Like the 2D case, only gradient refractive index (GRIN) materials are needed in the design. The material parameters of the whole cloak are obtained by rotating the refractive index profile in the 2D situation around the axis of the device ($z$ axis in the figure). In our design, the GRIN material was realized by multilayered dielectric plates with drilled inhomogeneous holes. According to the effective medium theory, the equivalent permittivity of the holey material can be estimated as $\varepsilon_{\text{eff}} = \varepsilon_0 f + \varepsilon_d(1 - f)$, where $f$ is the filling ratio of the holes that can be adjusted by the size of the holes.

Figure 11 shows the simulated and measured electric fields for the parallel-polarized incidence in the far region. It can be seen that the measured (Figures 11g–11i) and simulated (Figures 11a–11c) results are in good agreement at the operating frequency of 10 GHz. Figures 11a and 11g indicate the wave incident on the flat ground plane produces a single-peak reflection at the mirror-reflecting direction. Figures 11b and 11h are the situations when the cone-shaped metallic cover is present. It is obvious that the perturbations are generated in the far field. However, the single-peak reflection is restored as if the ground plane were flat when the metallic structure is covered by the designed 3D cloak, as shown in Figures 11c and 11i. In order to demonstrate the wide-band characteristics of the designed ground-plane cloak, measurements at the frequencies of 9 GHz and 12 GHz are carried out, as shown in Figures 11d–11f and Figures 11j–11l, respectively. Besides, the similar results are observed when illuminated with

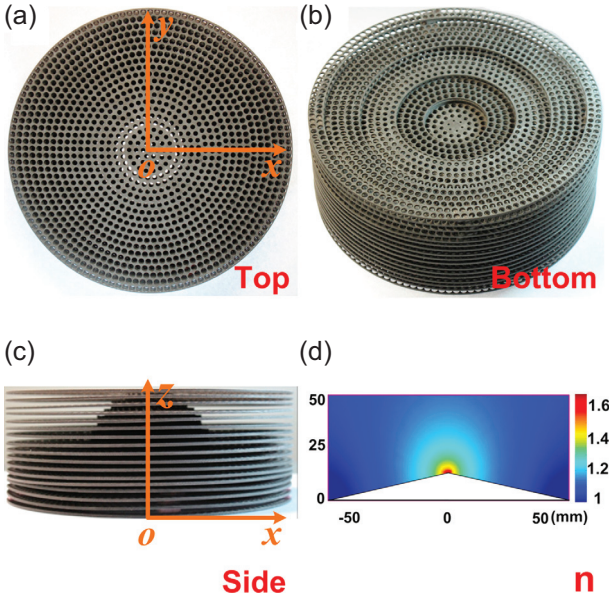


**Figure 10.** 3D microwave ground-plane cloak and its refractive index distribution. (a) Top view of the cloak. (b) Bottom view of the cloak. (c) Side view of the cloak. (d) The distribution of refractive index in the $x$–$z$ plane. Reprinted by permission from Macmillan Publishers Ltd: [41], copyright (2010).

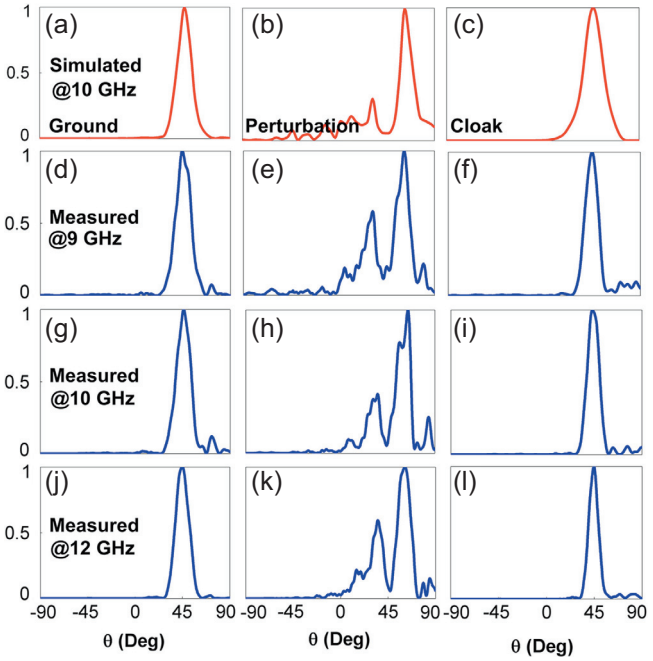


**Figure 11.** The simulated and measured electric fields in the far region. The fields are shown at different frequencies under the incidence of parallel-polarized electric field emitted from the metamaterial lens antenna. $\theta$ is the incidence angle. (a–c) Simulated results for the three situations at 10 GHz. (d–f) Measured results for the three situations at 9 GHz. (g–i) Measured results for the three situations at 10 GHz. (j–l) Measured results for the three situations at 12 GHz. Reprinted by permission from Macmillan Publishers Ltd: [41], copyright (2010).

perpendicular-polarized electric field. All above experimental results confirms the correctness of our design through drilling materials. It is obvious that good cloaking effects are achieved using the 3D cloak in a broad frequency band.

## 6 DC cloak

Like time-varying EM fields, static/steady electric/magnetic fields also play an important role in scientific sectors. As has been mentioned above, using transformation optics and metamaterial technology, various novel EM devices have been made possible, especially those on invisibility cloaks. However, only a few works are reported on invisibility cloaks and metamaterials for static/steady fields [57–62]. In 2012, our group presented the first experimental demonstration of a dc electric cloak for steady current fields using TO theory. The dc cloak was realized with a resistor network [17], as demonstrated in Figure 12.

For the steady electric fields and currents in a conducting medium, Maxwell's equations still hold. However, the constitutive equation is $\mathbf{J} = \sigma\mathbf{E}$, where $\sigma$ is the conductivity. As a result, the material transformation in the TO frame also goes for conductivity. For the realization of a 2D dc cloak, the linear transformation in cylindrical coordinate system was adopted, as used by Pendry's group [38]. Then, using TO, the transformed conductivities for the invisibility cloak can be written as

$$\bar{\sigma}' = \Lambda\left[\frac{\rho'-a}{\rho'}, \frac{\rho'}{\rho'-a}, \frac{\rho'-a}{\rho'}\left(\frac{b}{b-a}\right)^2\right]\bar{\sigma}. \qquad (9)$$

Where, $\Lambda$ represents a diagonal tensor. Again, inhomogeneous and anisotropic electrical conductivities are needed. As we all know, the required conductivities are difficult to be realized with natural materials. However, they can be readily emulated by using a resistor network.

Figure 13a illustrates the continuous conducting material plate (with the conductivity $\sigma$ and thickness $h$) discretized by the polar grid. Based on Ohm's law, each elementary cell in the grid can be implemented by two different resistors, one in the radial direction, and the other in the tangent direction, which can be expressed as

$$R_\rho = \frac{\Delta\rho}{\sigma_\rho \rho \Delta\varphi h}, R_\varphi = \frac{\rho\Delta\varphi}{\sigma_\varphi \Delta\rho h}. \qquad (10)$$

In which, $\Delta\rho$ and $\Delta\varphi$ are step lengths in the radial and tangential directions, respectively. Hence, different resistors in radial and tangential directions can be adopted to realize the anisotropic conductivity tensor, as show in Figure 13b.

Figures 14a and 14b present the simulated voltage distributions when a dc cloak works, which is used to hide a defect in a conducting medium. In the figure, the concentric circles represent the ideal equipotential lines for a point source. Figures 14c and 14d show the measured results when the central region is

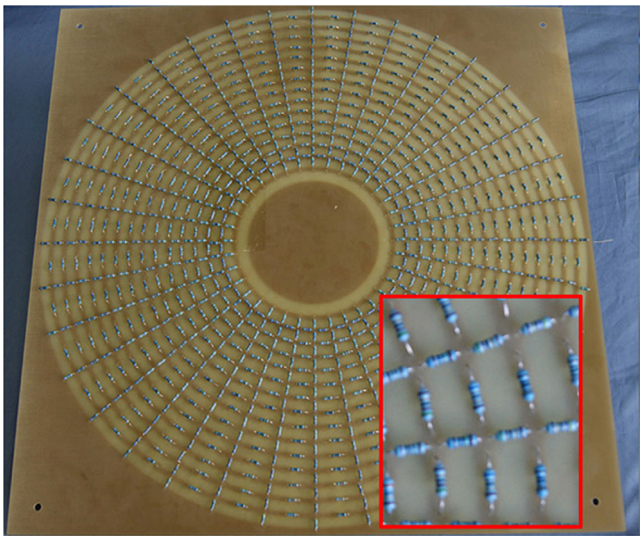

**Figure 12.** The fabricated dc electric cloak with an enlarged view for details. Reprinted (figure) with permission from reference [17] Copyright (2012) by the American Physical Society.

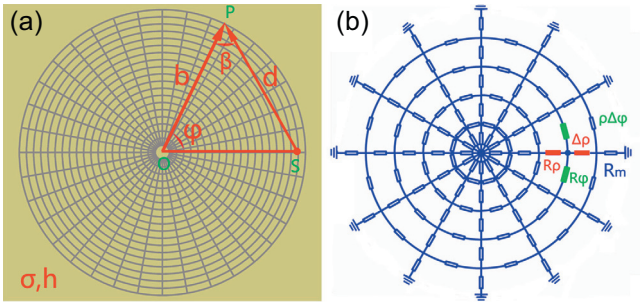


**Figure 13.** A conducting material plate (a) and its equivalent resistor network (b). Reprinted (figure) with permission from reference [17] Copyright (2012) by the American Physical Society.

cloaked. It is obvious that the potential distributions restore to the original concentric circles, as if no defect exists. Hence, the cloaked region can be protected from being detected. The comparison between the measured and the simulated results shows that they have good consistency. Though there is a tiny difference, it is mainly induced by the deviations between calculated and actually used resistors, and the distorted resistor distributions by manual soldering process. Hence the fabricated dc cloak has nearly perfect cloaking performance.

It seems that the dc cloaking has nothing to do with scattering manipulation. However, we remark that it represents a large number of applications using the "TO + metamaterial" frame, based on Laplace's equation. These applications include thermal cloaking, illusion and manipulation, and even acoustic cloaking, illusion and controlling. Though "scattering" does not apply or directly apply to these applications, similar methodologies can be borrowed in various designs [20, 63–69].

## 7 Mantle cloak: Invisibility induced by a surface

In recent years, metasurface [70] has attracted much attention, which can manipulate the phase, polarization and propagation mode of EM waves flexibly. Metasurface is an ultra-thin, 2D surface composed of arrays of metamaterial units. It has a series of fascinating EM properties by controlling the phase gradient or through impedance tuning, and can be used to design various EM devices [71–75]. Figure 15 shows a schematic mantle cloak from Alu's group [42], which is a patterned metasurface producing cloaking effect in a very thin geometry. In this design, the total scattering are greatly reduced by inducing suitable surface currents on the metasurface, which is readily achieved by tailoring its effective surface impedance with proper patterns. Besides, this mantle cloak is based on non-resonant units, having advantages like ultrathin structure, low loss and wide bandwidth, etc.

In the design of this mantle cloak, a patterned metallic surface composed of subwavelength periodic structures is adopted, whose EM behavior may be effectively described by an averaged surface impedance $Z_s = R_s - iX_s$. The relations between the averaged tangential electric field at the surface $E_{\tan}$ and the averaged induced surface current $J$ can be expressed as: $E_{\tan} = Z_s J$. This assumption is valid as long as the periodic pattern on a metallic surface is smaller than the wavelength of operation. In their work, the Mie scattering theory [76] was used to analyze the scattering problem, and the metasurface itself comes into the problem through impedance boundary conditions, i.e.

$$E_t|_{\rho=a_c^+} = E_t|_{\rho=a_c^-} = Z_s\left(H_t|_{\rho=a_c^+} - H_t|_{\rho=a_c^-}\right). \tag{11}$$

When illuminated by the plane waves, both TE and TM modes will be excited by the object and the cloak. To greatly suppress the scattering, one needs to minimize the dominant TM or TE modes in the scattered waves. Through rigorous calculation, the requirement for suppression of the $n$th TM mode is obtained, which requires the cancellation of the following determinant [42]:

*see the Equation (12) in the next page.*

For the TE mode, similar terms can be obtained by using the principle of duality. In the quasi-static limit, for which ($k_0 a_c \ll 1$), the dominant contribution to scattering is given by the $n = 1$ dominant mode, and the approximate conditions for cloaking in the two polarizations may be written in an closed form, which are

$$\begin{aligned} \mathrm{TM}: X_s &= \frac{2[2+\varepsilon-\gamma^3(\varepsilon-1)]}{3\gamma^3\omega a\varepsilon_0(\varepsilon-1)} \\ \mathrm{TE}: X_s &= \frac{\omega a\mu_0[2+\mu+2\gamma^3(\mu-1)]}{6\gamma^3(\mu-1)} \end{aligned} \tag{13}$$

From equation (13) we can see, both the TE and TM mode can be suppressed by proper choice of the surface reactance [77]. When the size of the object is comparable to the wavelength, a perfect mantle cloak can be designed by using equation (13).

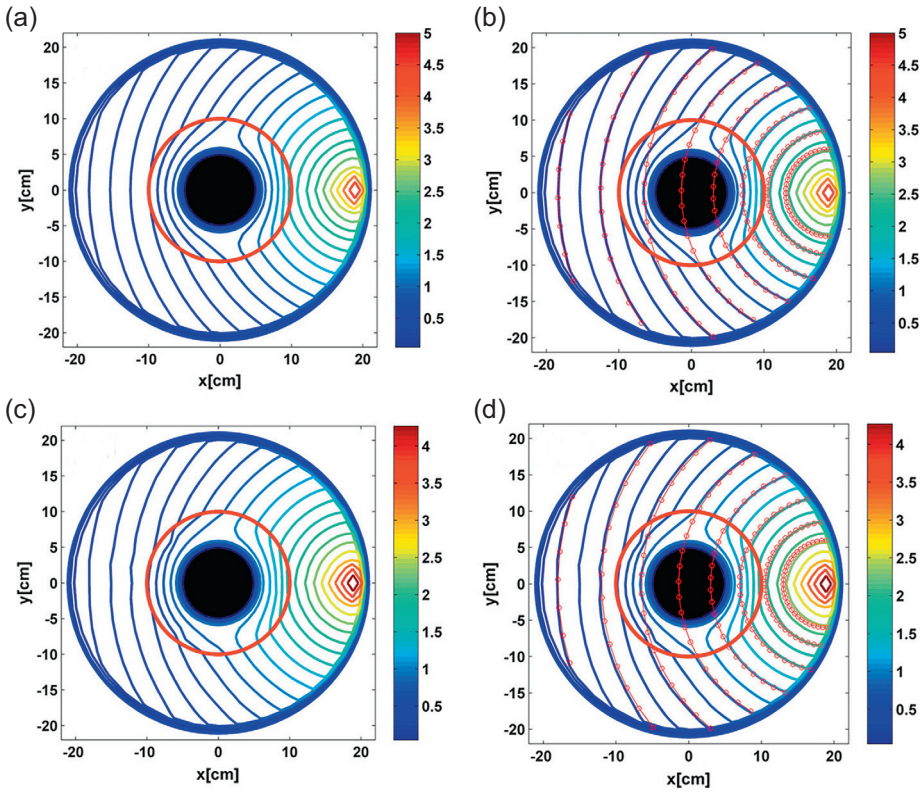


**Figure 14.** The simulated (a), (b), and measured potential (voltage) distributions (c), (d), when the dc cloak exists to hide the central region. Note that the concentric circles denote the ideal equipotential lines. Nearly perfect cloaking effect is observed. Reprinted (figure) with permission from reference [17] Copyright (2012) by the American Physical Society.

Figure 16 shows the variation of the total SCS with the surface reactance of a mantle cloak, which is covered on the surface of a sphere with permittivity $\varepsilon = 10$ and diameter $2a = \lambda_0/5$, and for different frequencies of operation.

When compared to the bare sphere represented by the thin dashed line, it is obvious that the total SCS can be reduced in a significant degree by choosing a proper surface reactance. It is also seen that for sufficiently large reactance values the patterned surface does not have any effect on the scattering. This is understandable since the limit of no surface is given by $X_s \to \infty$. Figure 16b demonstrates that for the special design ($a_c = 1.1a$), a very large of reduction of scattering can be achieved with a specific surface reactance (175 Ω) in a wide bandwidth, which shows that a suitably designed mantle cloak can achieve significant scattering reduction over a large frequency range.

It is obvious that a mantle cloak with suitable surface reactance may largely reduce the scattering and restore unperturbed planar wavefronts around the cloak. Compared to the transformation-based cloaks that completely insulate the object, the field can penetrate inside the sphere, and may also provide the possibility to sense and extract the signal inside the mantle device without significantly perturbing the surrounding EM field. Moreover, the cloak has a wider bandwidth. The main disadvantage of the design is that the size of the cloaked object cannot be very large. It is expected that a multilayered surface, or an anisotropic one, may provide more degrees of freedom, suppress higher modes, and lead to better performances.

## 8 Ultra-thin carpet cloak and "skin" cloaking with a metasurface

The cloaks designed with transformation optics are seriously challenged by the very complex material properties [38]. Carpet cloaks based on quasi-conformal mapping can greatly reduce the complexity of material, and these devices are placed on top of object on the ground against overhead

$$U_n^{\mathrm{TM}} = \begin{vmatrix} j_n(ka) & j_n(k_0a) & y_n(k_0a) & 0 \\ [kaj_n(ka)]'/\varepsilon & [k_0aj_n(k_0a)]' & [k_0aj_n(k_0a)]' & 0 \\ 0 & j_n(k_0a_c) + [k_0a_cj_n(k_0a_c)]'/(i\omega\varepsilon_0a_cZ_s) & y_n(k_0a_c) + [k_0a_cy_n(k_0a_c)]'/(i\omega\varepsilon_0a_cZ_s) & j_n(k_0a_c) \\ 0 & [k_0a_cj_n(k_ca_c)]' & [k_0a_cy_n(k_0a_c)]' & [k_0a_cj_n(k_0a_c)]' \end{vmatrix} \quad (12)$$

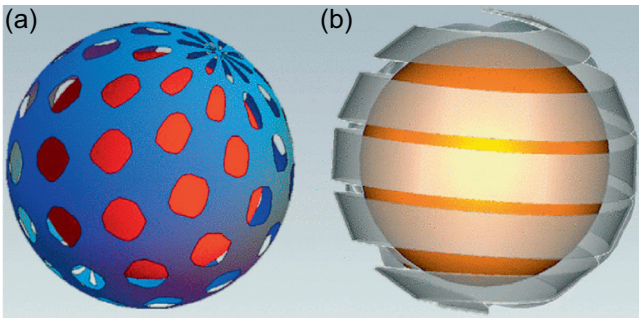


**Figure 15.** Examples of patterned metallic geometries that may realize a mantle cloak. Reprinted (figure) with permission from reference [42] Copyright (2009) by the American Physical Society.

detection. However, in most cases, the shell is too thick for practical applications [78]. In this regard, metasurface provides another route for designing ultra-thin carpet cloaks.

Figure 17 is an ultra-thin carpet cloak that we proposed in 2013 [43]. The cloak is a tent-like structure made of two metasurfaces (only one is shown due to the symmetry of the structure). When illuminated by EM waves from above, the reflected waves will propagate along the original way as if the EM wave is incident on a flat ground plane.

For the realization the ultra-thin carpet cloak, the reflection phase of the metallic patches on the structure need to be carefully tuned. As shown in Figure 17, in order to cancel the optical path difference corresponding to the adjacent units $(4\pi/\lambda_0)\ p\ \sin\ \theta$, an additional phase change between the neighboring units should be:

$$\Delta\phi = 2k_0\Delta s = (4\pi/\lambda_0)p\sin\theta \tag{14}$$

Based on the metallic "H" patterns, the 2D ultrathin carpet cloak was implemented, and the experimental measurement at microwave frequencies is performed. Numerical and experiment results all confirm the correctness of the idea [43]. Based on the similar theory, Alù and other scholars also designed similar 2D and 3D carpet cloaks [79].

In 2015, Hsu et al. rigorously analyzed and got the required phase distribution of an arbitrarily-shaped 2D carpet cloak [80], which was given in equation (15):

$$\Phi(x) = 2k_0 z(x)\cos(\theta_G) + \text{const}, \tag{15}$$

where, $\theta_G$ is the incidence phase, $z(x)$ is the shape function of the carpet, and const is the reflection phase by ground. They also presented an implementation method based on dielectric resonant unit, which makes the device work at a higher frequency.

Also in 2015, Zhang's group proposed and verified a 3D skin cloak in the optical frequency [81]. This cloak can hide multiple bumps and dents on the ground from being detected. In the design, reflected phase from the irregular surface is manipulated by nano antenna arrays. After manipulation, the reflection phenomenon is similar to specular reflection, and hence the cloak is achieved. Figure 18 shows the experimental results of the extremely thin 3D invisibility skin cloak [81].

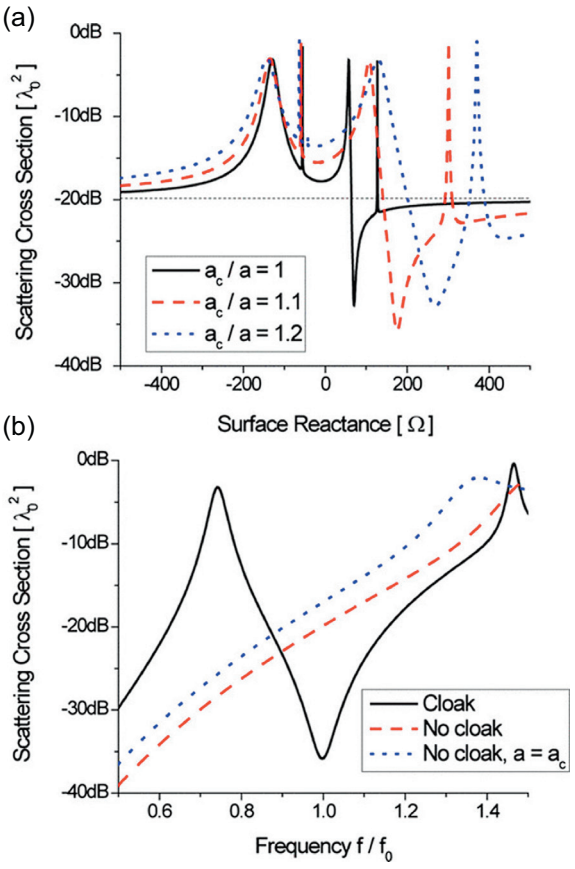


**Figure 16.** Variation in the total scattering cross-section of a dielectric sphere with $\varepsilon = 10$ and $2a = \lambda_0/5$ with: (a) the surface reactance of a mantle cloak; (b) the normalized frequency of operation for a cloak with $a_c = 1.1a$ and $X_s = 175\ \Omega$. Reprinted (figure) with permission from reference [42] Copyright (2009) by the American Physical Society.

The ultra-thin property is an outstanding advantage of skin cloaks as compared to its bulky counterpart. However, the disadvantage is also very obvious, i.e. its directional property, making the cloak effective in only a particular direction. Once the incident direction is changed (for the probing waves), the stealth performance dropped significantly. However, with the development of dynamically controllable metamaterial, the realization of a new skin cloak, whose reflected phase distribution can be modulated in a real-time manner according to the incident EM waves, is not impossible.

## 9 Scattering control with digital and programmable metasurface

In 2014, the concepts of coding metamaterials and programmable metamaterials were proposed to control the scattering and radiations of EM waves using digital coding particles [44]. In essence, they are controllable EM metasurfaces. A typical unit cell and a digital metasurface are shown in Figure 19. As we have mentioned earlier, metasurface, as a new type of 2D artificial structure, is made of arrays of subwavelength units which are arranged according to certain

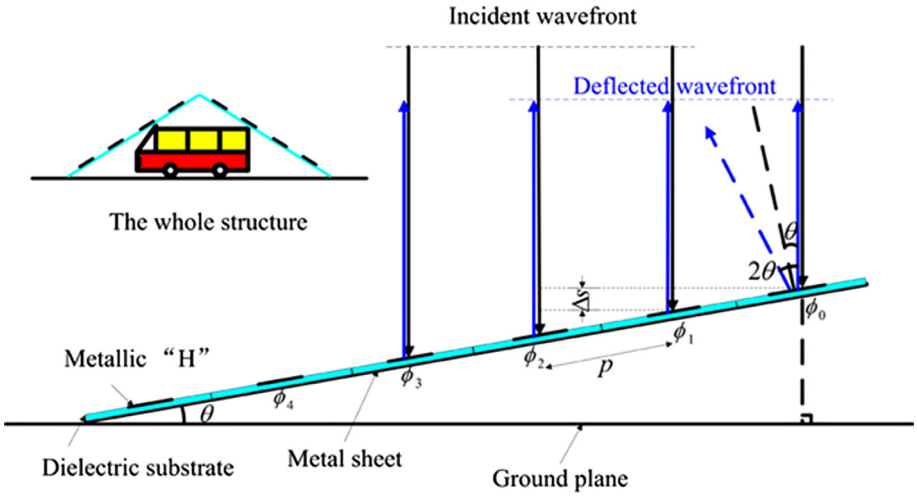


**Figure 17.** The schematic of an ultrathin carpet cloak and its working mechanism. Reprinted from reference [43] with the permission of AIP Publishing.

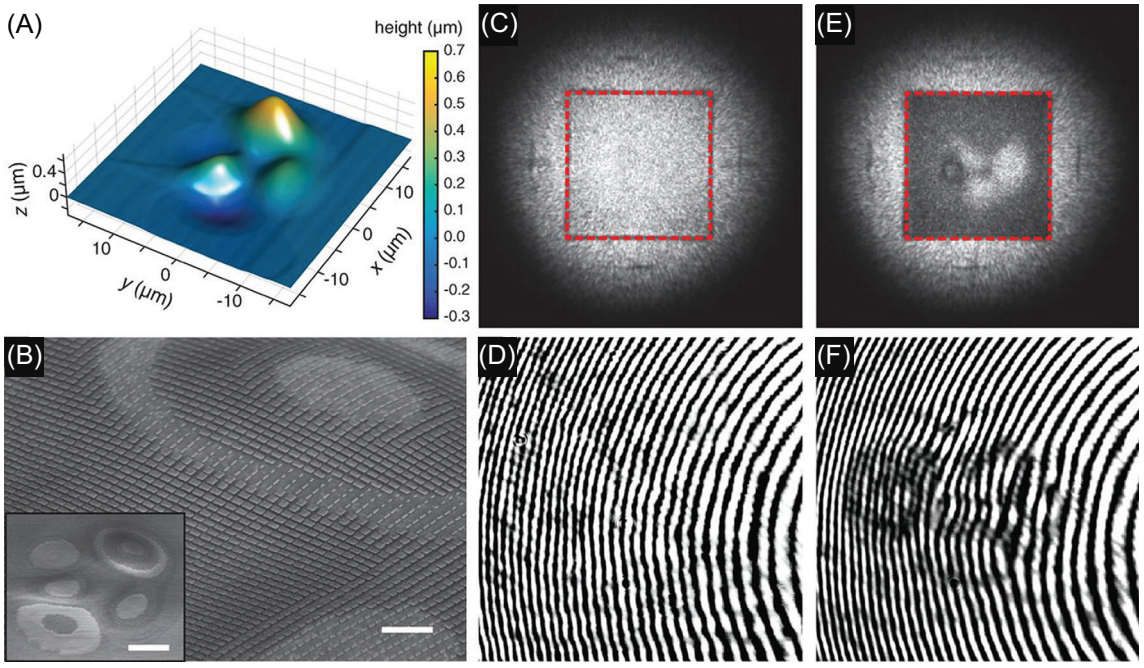


**Figure 18.** An ultrathin invisibility skin cloak for visible light. (A) An AFM image of a 3D arbitrarily shaped object that includes multiple bumps and dents. (B) A SEM images of the object onto which a metasurface skin cloak has been fabricated. (C) The obtained reflection image when the cloak is on; (D) The interference image when the cloak is on; (E) The obtained reflection image when the cloak is off; (F) The interference image when the cloak is off. From reference [81]. Reprinted with permission from AAAS.

rules. Each unit cell can realize specific reflection and/or transmission phase. Hence, EM waves can be manipulated flexibly by controlling the phase of the units. In most cases, these phases approximately cover an interval between $[0, 2\pi]$. Due to the discrete nature of the unit cells, only a finite number of phases are selected in the interval and realized using specific unit cells. Then, if we encode these discrete values in binary numbers, the digital metamaterial (unit) is obtained, which differs from the analog counterpart due to the limited number and discrete phase values. The so-called coding metamaterial can be obtained when the corresponding digital units are arranged in a certain pattern. If the field programmable gate array (FPGA) is used for dynamically controlling the arrangement of these units, the programmable metamaterials will be obtained. It can be seen that, with the development of electronics, control theory and computer technology, the implementation of arbitrarily programmable metamaterial is almost within reach.

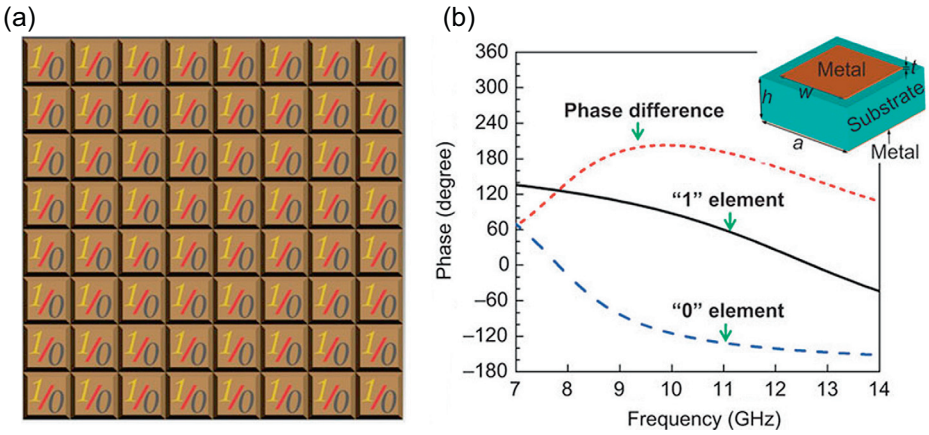


**Figure 19.** The 1-bit digital metasurface (a) and a typical unit cell together with its phase responses at different frquencies (b). The 1-bit digital metasurface is composed of only two types of elements: "0" and "1". Reprinted by permission from Macmillan Publishers Ltd: [44], copyright (2014).

To facilitate understanding, we begin with the simplest case of phase-coding, i.e. one-bit coding, in the context of a reflectarray. "One-bit" coding metamaterials compose of only two types of unit cells, with 0 and $\pi$ reflected phase responses, respectively (named as "0" and "1" elements, please refer to Figure 19). Then, the control of EM wave can be realized by arraying "0" and "1" elements with regular patterns on a 2D surface. For actual configurations, we can arrange the unit cells in a 0000. . ./0000. . . pattern, which means "0" elements are arrayed in both $x$ and $y$ directions; another pattern is 010101. . ./010101. . ., which indicates alternating 0 and 1 elements are patterned in $x$ direction while the arrangement in $y$ direction remains unchanged; of course, the third pattern can also be adopted, i.e. 01010101/1010101, and this suggests alternating arrangements in both $x$ and $y$ directions. For the first arrangement, there is no phase gradient in $x$, $y$ directions since the metasurface is composed of the same unit. As a result, the normally incident beam will mainly be reflected to original directions, which is similar to specular reflection, as shown in Figures 20a, 20d and 20g. While for the second pattern, the alternating arrangement of "0" and "1" elements in $x$ direction introduces a $\pi$/unit phase gradient. Then, based on generalized Snell's law [70], the normally incident beam will be reflected to two symmetrically oriented directions in the $xoz$ plane, instead of its original directions, as illustrated in Figures 20b, 20e and 20h. Similarly, when a phase gradient is introduced in $y$ direction as well as $x$ direction, as is done in the third scheme, the normally incident beam will mainly be reflected to four symmetrically oriented directions, as demonstrated in Figures 20c, 20f and 20i. It can be seen that due to the introduction of discretization and coding scheme, the metasurface has more degrees of freedom for realizing more complex functions. It is quite obvious that when "0" and "1" units are arranged in random distributions, the reflected EM waves will become disordered, and then the diffuse reflection is obtained. In this case, as a matter of fact, the 2D EM metasurface is a kind of random surface.

For the "1 bit" case, if a control mechanism is integrated into the unit design, one can get a programmable metasurface using this tunable unit cells. A specific realization and control method are also given by our group too [44], as illustrated in Figure 21. The two quasi rectangular units are linked by a varactor, whose bias voltage are provided by two metal strips on the back surface of the PCB through two via holes. When the voltage between the metal strips is 3.3 V, the unit is in "on" state, corresponding to phase "1"; however, when the bias voltage of the metal strips is 0 V, the unit is in "off" state, corresponding to phase "0". Therefore, the units' working state can be controlled by modulating the voltage on metal strips. Through the application of FPGA, we also realized a specific programmable EM metamaterials, capable of realizing the above patterns, and experiment results confirm the correctness of the design.

Besides, the "multiple-bit" coding metamaterial can also be designed by simply adding more phases in the cell design. For example, the "2-bit" metamaterial is composed of four types of unit cells with phase difference close to 90°, (coded as "00", "01", "10" and "11" elements). EM waves can be controlled by regulating the distribution of "00", "01", "10" and "11" with certain rules. Similarly, when metasurface is controlled by FPGA, the programmable metamaterials can be realized. If they are controlled by FPGA in a real-time manner, a variety of functions can be achieved, such as single-beam, multi-beam, beam scanning, and active cloaking, etc. Predictably, coding and programmable metamaterials lay a solid foundation for the future development of intelligent radar and other intelligent systems.

## 10 Scattering manipulation with optimized multilayer structures

Scattering manipulation schemes, whether they are based on TO or metasurfaces, generally require metamaterials for realization due to material limitations in nature. As a result, the weak points for the current-stage metamaterials are also brought into the scheme (e.g. narrow bandwidth, relatively large loss, and polarization sensitivity). In this regard, a novel scheme using natural materials or their combinations seems much desirable and plausible. However, one has to use

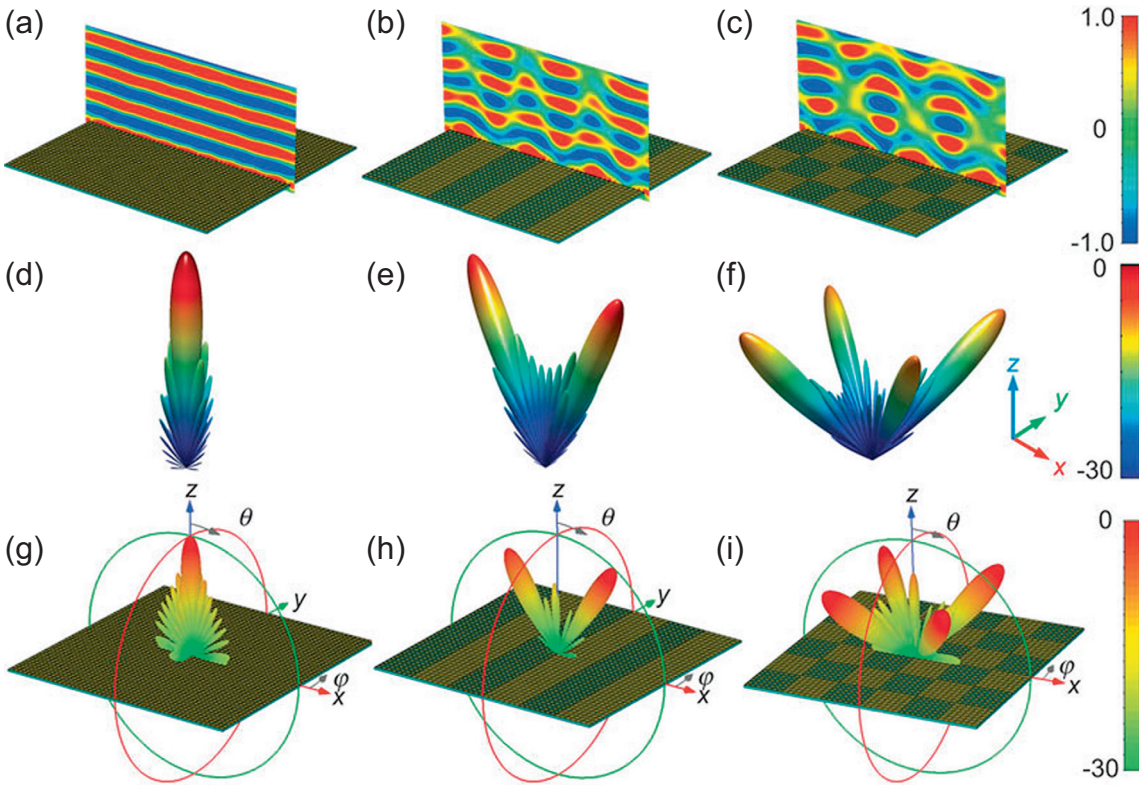


**Figure 20.** Full-wave simulation results of 1-bit periodic coding metasurfaces. (a–c) The 1-bit metasurface structures with periodic coding sequences: (a) 000000. . ./000000. . ., (b) 010101. . ./010101. . ., (c) 010101. . ./101010. . ., and their corresponding near-field distributions. (d–f) The analytical results of the corresponding coding sequences. (g–i) The full-wave simulation results of the corresponding coding sequences. Reprinted by permission from Macmillan Publishers Ltd: [44], copyright (2014).

"quantity" for the sake of "quality", i.e. to get more "degrees of freedom" to deal with the complexity and add flexibility in this scenario. A very simple route is to use a multilayered shell structure, whose geometrical size and EM parameters can be optimized in a controlled manner, so as to give the proper EM response. Genetic algorithm [82], a heuristic optimization method, can usually do the work, since the controllable parameters for each layer can be naturally coded and connected together, giving rise to a "chromosome". The evolution of the chromosome eventually leads to an optimized design. However, other optimization methods may also be utilized for this problem.

The first example is for the cloaking application. In 2009, Popa and coworkers present a method to reduce the scattering from arbitrary objects by surrounding them with multilayers of homogeneous and anisotropic materials [45]. They used an optimization procedure, i.e. Broyden-Fletcher-Goldfarb-Shanno (BFGS) method, which is already implemented in software tools such as MATHEMATICA and MATLAB, to find the material parameters for each layer. The authors showed that an optimized three-layer shell can reduce the maximum scattering of an object by as much as 15 dB more than a 100-layer realization of a coordinate transformation cloaking shell.

Though the authors argued that the method can be used for cloaking arbitrary object, they illustrated the procedure by using a 2D cylindrical object. As illustrated in Figure 22, a PEC cylinder is wrapped by an M-layered shell and illuminated by a TE polarized plane wave (electric field in the $z$ direction). The inner and outer radii of the shell are $a$ and $b$, respectively. Each layer is supposed to have the same thickness, of course, this is not necessary in other cases. Due to the simplicity of the current problem, the scattered field for this composite structure can be easily obtained using the Mie scattering theory [76], which is

$$E_{sc} = \sum_{n=0}^{\infty} A_n H_n^{(2)}(k_o r)\cos n\phi. \tag{16}$$

The radar cross section per unit length, also known as scattering width (SW) of the structure, is defined as $\sigma(\phi) = 2\pi R|E_{sc}(\phi, R)/E_{\text{inc}}|^2$, where $R$ is a large distance from the cylindrical axis, and $E_{\text{inc}}$ is the amplitude of the incident wave. Because of the TE polarization, only material parameters $\varepsilon_z^{(1\ldots M)}, \mu_r^{(1\ldots M)}, \mu_\phi^{(1\ldots M)}$ for each layer are concerned, and the changes of these parameters will definitely modify the scattering width. Hence, the authors expect to minimize the objective function, i.e. SW, by optimizing these material parameters.

In their design procedure, the starting points for the material parameters are

$$X_0 = \left(\varepsilon_{z,0}^{(1\ldots M)}, \mu_{r,0}^{(1\ldots M)}, \mu_{\phi,0}^{(1\ldots M)}\right), \tag{17}$$

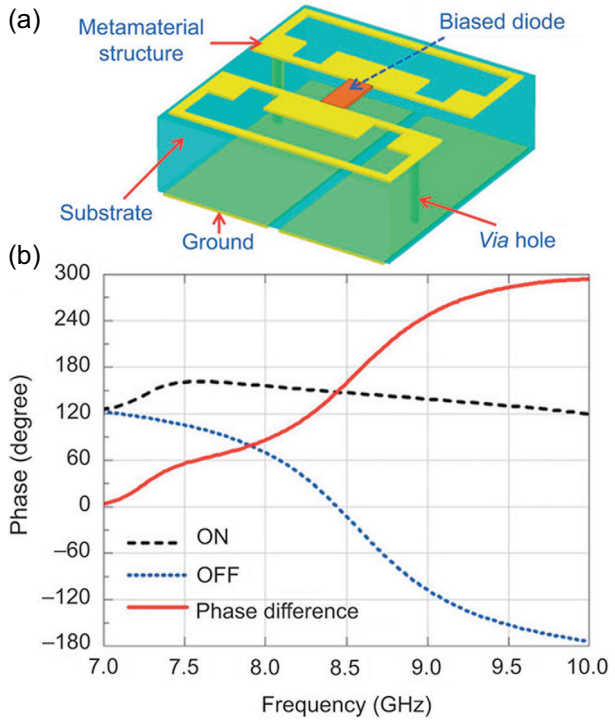


**Figure 21.** Controllable 1-bit unit. (a).The structure of metamaterial particle, which behaves as "0" and "1" elements when the biased diode is "OFF"and "ON". (b) The corresponding phase responses of the metamaterial particle at different frequencies. Reprinted by permission from Macmillan Publishers Ltd: [44], copyright (2014).

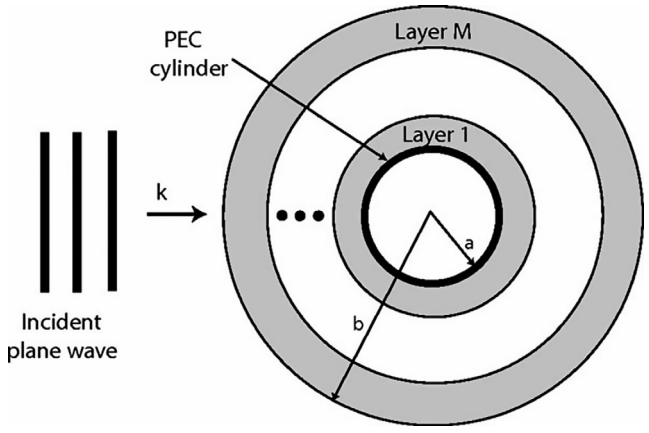


**Figure 22.** Cylindrical perfect electric conductor surrounded by a multilayer shell and illuminated with a plane wave. The input and output radii of the shell are $a$ and $b$, respectively. Reprinted (figure) with permission from reference [45] Copyright (2009) by the American Physical Society.

**Table 1.** Optimized material parameters for the three-layer cloak. Reprinted (table) with permission from reference [45] Copyright (2009) by the American Physical Society.

| | Initial guess | | | Optimized parameters | | |
|---|---|---|---|---|---|---|
| Layer | $\varepsilon_z$ | $\mu_r$ | $\mu_\phi$ | $\varepsilon_z$ | $\mu_r$ | $\mu_\phi$ |
| 1 | 1.60 | 0.021 | 47.15 | 3.32 | 0.006 | 47.21 |
| 2 | 4.61 | 0.061 | 16.38 | 6.06 | 0.039 | 16.88 |
| 3 | 7.40 | 0.098 | 10.23 | 7.99 | 0.10 | 10.63 |

which is the discrete values by the TO design. By utilizing the BFGS method, the authors successfully got the optimized parameters for the $M = 3$ case, i.e. only three layers are used in the optimization. Table 1 lists the output parameters together with the initial guess.

The performance of the design is given in Figure 23. For comparison, the discrete implementation of the TO-based cloak design with different layers is also provided in the figure. It is quite obvious that the optimized design gives rise to the best performance. In this case, the maximum scattered field is approximately 15 dB smaller for the optimized three-layer cloak than for the 100-layer discretization of the coordinate transformation cloak.

As has been pointed out earlier, constraints for material parameters can also be incorporated into the optimization procedure, so as to lower the implementation difficulties. In this regard, Popa and coworkers demonstrated a nonmagnetic multi-shell design for the TM polarized plane waves, and for the same object. Figure 24a shows the optimization results. Again, compared with the analytical nonmagnetic design and the three-layer discretization of the analytical version, the optimized three-layer design leads to the lowest scattering. Figure 24b illustrates the simulated near field distribution, similar conclusions can be made. The above observation once again validates the correctness and advantage of the optimization method.

Besides cloaking, optimized multilayer structure can also be used for the magnification of an object, i.e. for super-scattering applications. In 2014, Mirzaei et al. [46] used genetic algorithm to design a realistic core-shell nanostructures with the super-scattering effect, which can be achieved at any desired wavelength. In their design, a three-layered long cylinder is studied, the core of which is silicon, and the exterior layers are silver and silicon, respectively. The exterior radius of the structure is fixed at 87 nm. Moreover, the material data are all obtained from the optical experiments. The goal of their work is to produce as much scattering as possible, when illuminated by a TM polarized wave. Then it is clear that the only remaining degrees of freedom are the radii of each layer, which are designated as $r_1$, $r_2$ and $r_3$, respectively. Mathematically speaking, this can be realized by maximizing the following function, i.e. the normalized scattering cross section

$$F_i(r_1, r_2, r_3) = \max\left\{\mathrm{NSCS}\left(\lambda_{\mathrm{opt}}, r_1, r_2, r_3\right)\right\}. \qquad (18)$$

where $\lambda_{\mathrm{opt}}$ is the prescribed optimum working wavelength. By using genetic algorithm, the authors successfully show two optimized designs, one working at 500 nm wavelength, and the other at 600 nm. The radii for these two configurations are {49, 78, 87} and {47, 66, 87}, respectively. Figure 25 shows the normalized scattering cross section of the two configurations, as well as the contributions from first three modes.

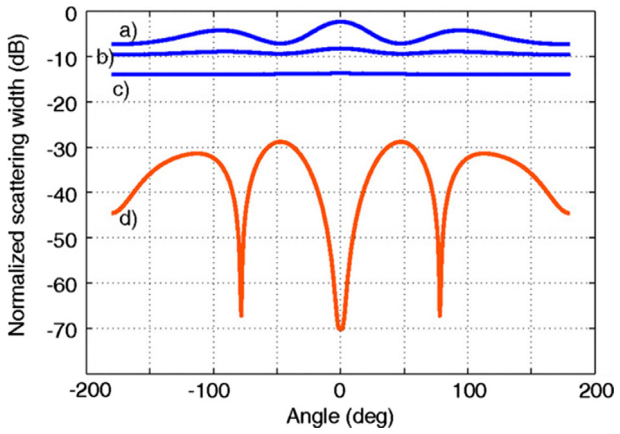


**Figure 23.** The scattering width normalized to the object diameter for the three-layer (a), nine-layer (b), and 100-layer (c) approximations of the analytical cloak compared to the optimized cloak (d). Reprinted (figure) with permission from reference [45] Copyright (2009) by the American Physical Society.

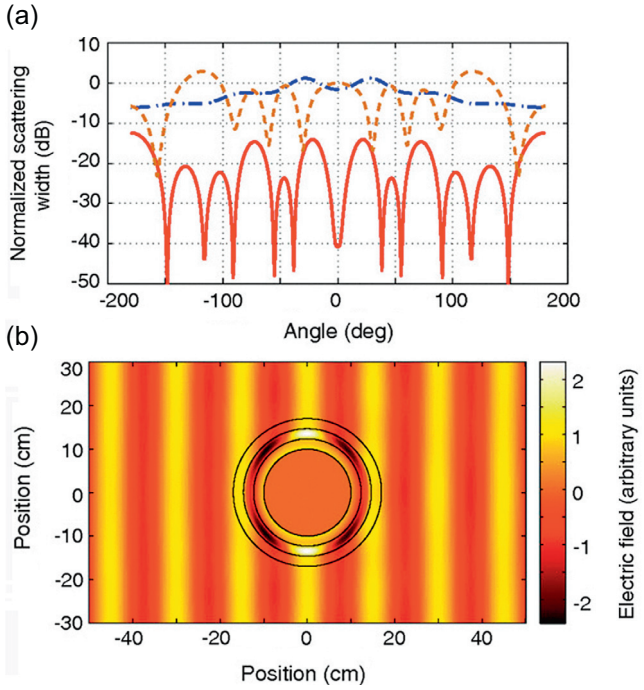


**Figure 24.** (a) The scattering width vs angle for the three-layer approximation of the analytical cloak (dash-dotted), nonmagnetic cloak (dashed), and three-layer optimized nonmagnetic cloak (solid). (b) The total fields inside and around the nonmagnetic optimized cloak. Reprinted (figure) with permission from reference [45] Copyright (2009) by the American Physical Society.

Clearly, the normalized scattering cross section reaches maximum at the predesigned wavelength, firmly validating the design. Far field radiation patterns for the two are also given in Figure 26, same conclusions can be made.

In the above design, all materials are naturally achievable, and the optimization process is on the geometrical size of each shell, hence it firmly shows the flexibility and practicability of

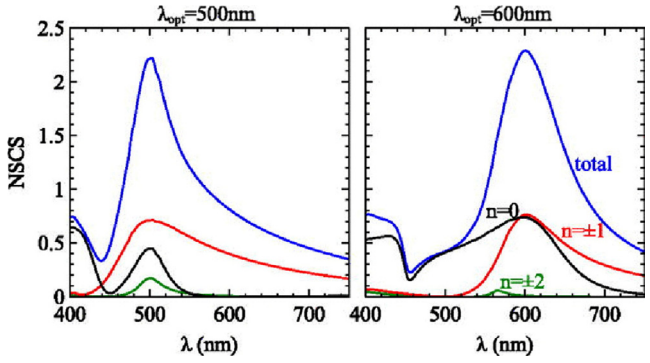


**Figure 25.** Spectrum of the NSCS of optimized superscattering structures at different wavelengths. Shown is the total cross-section, as well as contributions of the first three modes. Reprinted from reference [46] with the permission of AIP Publishing.

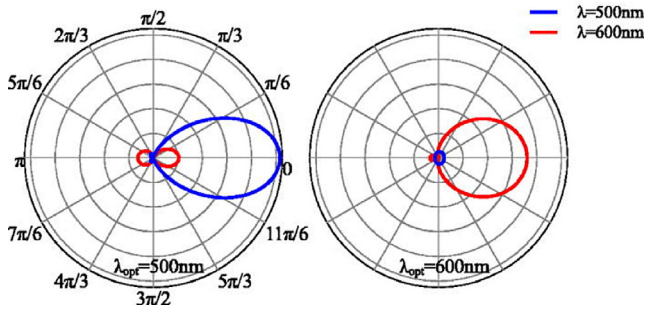


**Figure 26.** Far field radiation pattern of structures optimized for different wavelengths. Both panels have the same radial tick steps. Reprinted from reference [46] with the permission of AIP Publishing.

the method and the structure. Based on similar ideas, cloaking devices using multilayered structures with homogeneous or inhomogeneous materials, for spherical or cylindrical objects, and with isotropic or anisotropic parameters, are also put forward and studied in the community [83–85]. Moreover, an experimental demonstration of a free-space cylindrical cloak was made by Chen et al. from Zhejiang University, China, in 2012 [86].

As the last example, we show how a multilayer structure can change the scattering features of a dielectric cylinder into a perfect electric conductor, for which one can call "illusion". Very recently, Hwang et al proposed an annular multilayer structure using alternating silicon and silicon dioxide layers along the radial direction [47]. In the design, the core has radius $a$ = 500 nm and the refractive index $n$ = 3.475 (silicon). There are ten periods in the radial direction and each period contains two dielectric mediums with refractive indices $n_1$ = 1.45 (silica) and $n_2$ = 3.475. The thickness for each dielectric is the same, which is 100 nm. Hence, the radius of the metamaterial cylinder is $b$ = 2500 nm. A TM polarized plane wave is incident on the cylinder and is scattered by the structure. They show that when the incident photon energy is about 1.2 eV, then the scattering feature of the composite structure is the same as that of Au and PEC, and only very small discrepancies can be observed in the forward direction.

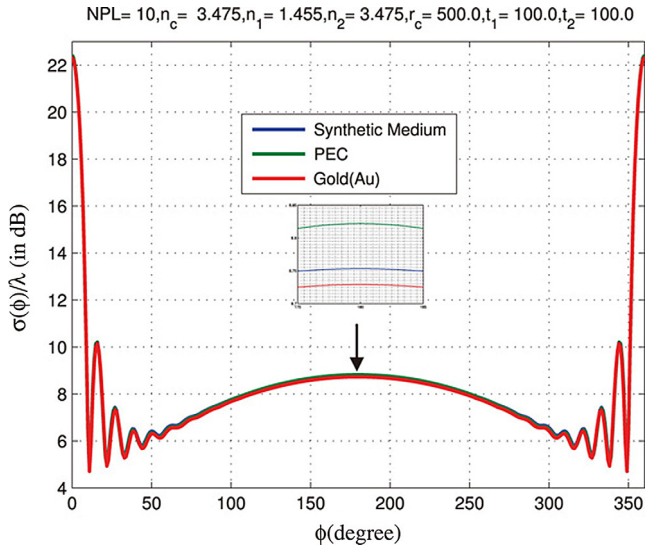


**Figure 27.** Variation of the normalized echo width against $\phi$ at 1.2 eV for the three materials, including a perfect electrical conductor, Au and the metamaterial. They share the same diameter of 2500 nm. From reference [47].

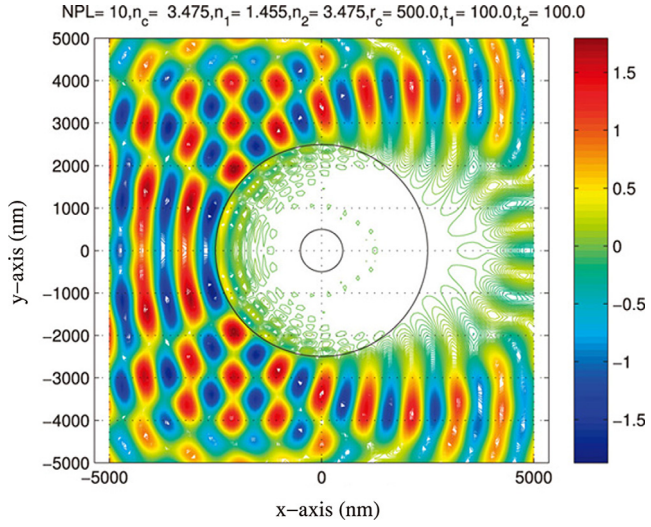


**Figure 28.** The distribution of the z-axis electric field component along the 2D plane. A plane wave with photon energies of 1.2 eV is incident on the structure, the real part of $E_z(x, y)$. From reference [47].

The normalized scattering width is shown in Figure 27. Please note that all three cylinders share the same radius, i.e. 2500 nm. Then, this result tells us that a dielectric cylinder is actually disguised as a gold one or a PEC cylinder. The near field distribution around the structure, as shown in Figure 28, again confirms the arguments. The only difference between the synthetic structure and the PEC cylinder is that the tangential electric field at the exterior boundary of the former does not vanish, as opposed to the latter case.

As a matter of fact, due to the periodic boundary conditions, the wave propagation along the radial direction can be rigorously predicted using Floquet-Bloch theorem. Then, the authors analytically obtained the eigenvalue problem for the problem concerned, and got the Brillouin diagram for the structure. As can be expected for other periodic structures, the multilayer structure was found to exhibit stop- and pass-bands, enabling total reflection in band-gap regions. For photon energy of 1.2 eV, it lies right in the band-gap regions. As a result, the "illusion phenomenon" is quite understandable since waves cannot propagate inside the structure due to large attenuations associated with band-gaps.

## Conclusions

In the present work, we have reviewed various devices and methods on scattering manipulations using metamaterials. Generally speaking, all of them involve a shell structure, though it may be bulky or slim, 2D or 3D, and multilayer or single layer. When used to cover the object, all these shell structures can modify the original scattering patterns in a pre-designed manner, like the invisibility, illusion, super-scattering, and abnormal scattering, etc. Though we have tried to cover as many schemes as possible, there are some devices and methods not mentioned in this review.

At the present stage, most devices only produce static manipulations, which means function of the device is fixed when fabricated. However, dynamic and real-time controls are emerging [87]. In this regard, the device has more than one functions on scattering manipulation, which can be dynamically controlled using "switches" embedded in the device. This switchability adds more flexibility for practical designs and will eventually lead to self-adaptive devices, i.e. devices that can change their functions according to different "environments".

Another way for scattering manipulation is the active scheme. Compared with passive methods reviewed in this work, this scheme involves lots of controllable sensors and emitters around the target. The core of the scheme is to sense the properties of incident waves and at the same time, manipulate the emitters according to calculations on the incident waves. The superimposed field can manifest different results like invisibility, illusion, and abnormal scattering, etc, in accordance with specific calculations [88]. However, we must note that the boundary between active devices [89] and the programmable/controllale metamaterial [44] is disappearing.

Moreover, there are still other methods excluded in this review, among which is the ray optics method, which depends on the usage of lenses for the control of the rays around the target [90–92]. Though work in an approximated way, these devices have the merit of large scale, wide bandwidth, and easy fabrication, etc.

On the other hand, novel metamaterials should be further studied and analyzed since they lay the physical foundation for device realization. In this regard, controllable/programmable metamaterial will be a very important direction. The controllability of metamaterial is the basic requirement for dynamic manipulation of the electromagnetic field. Their controllable properties can make the manipulation of EM fields much simpler, smarter and more flexible. Besides, the working bandwidth poses another problem for practical applications,

especially for those approaches working with the resonance mechanism. Hence, it is also an important research direction to broaden the working bandwidth of metamaterials. In addition to this, metamaterials based on graphene will see lots of applications in the near future. Those metamaterials are ultra-thin 2D films with an atomically-thick thickness, and the electromagnetic properties can be flexibly tuned using electric, magnetic and chemical methods.

In one word, no matter what scheme is applied, it will depend on the realization of novel metamaterials with controllability, flexibility, wide bandwidth, low loss, and compactness, etc. However, Rome was not built in one day! There is still a long way to go to convert research results drastically into productive forces. The existing problems and chanlleges will definitely propel the research on matematerials to a higher level.

*Acknowledgements.* This work was supported by National Natural Science Foundation of China (61302018, 61401089, 61401091, 61571117, 61501112, 61501117, 61138001), National Instrumentation Program (2013YQ200647), 111 Project (111-2-05), and Natural Science Foundation of the Jiangsu Province (BK2012019). Z.L. Mei acknowledges the Fundamental Research Funds for the Central Universities (Grant No. LZUJBKY-2015-k07) and the Open Research Funds of State Key Laboratory of Millimeter Waves (Grant No. K201717).

## References

1. V.G. Veselago, The electrodynamics of substances with simultaneous negative values of $\varepsilon$ and $\mu$, Sov. Phys. Usp. 10 (1968) 509–514.
2. R.A. Shelby, D.R. Smith, S. Schultz, Experimental verification of a negative index of refraction, Science 292 (2001) 77–79.
3. S. Xi, H. Chen, T. Jiang, L. Ran, J. Huangfu, B.I. Wu, J.A. Kong, M. Chen, Experimental verification of reversed Cherenkov radiation in left-handed metamaterial, Phys. Rev. Lett. 103 (2009) 194801.
4. S.N. Galyamin, A.V. Tyukhtin, A. Kanareykin, P. Schoessow, Reversed Cherenkov-transition radiation by a charge crossing a left-handed medium boundary, Phys. Rev. Lett. 103 (2009) 194802.
5. A. Lakhtakia, Positive and negative Goos-Hanchen shifts and negative phase-velocity mediums, Int. J. Electron. Commun. 58 (2003) 229–231.
6. T.J. Cui, X.Q. Lin, Q. Cheng, H.F. Ma, X.M. Yang, Experiments on evanescent-wave amplification and transmission using metamaterial structures, Phys. Rev. B 73 (2006) 245119.
7. J.B. Pendry, Negative refraction makes a perfect lens, Phys. Rev. Lett. 85 (2000) 3966–3969.
8. D.R. Smith, J.J. Mock, A.F. Starr, D. Schurig, Gradient index metamaterials, Phys. Rev. E 71 (2005) 036609.
9. M. Silveirinha, N. Engheta, Tunneling of electromagnetic energy through subwavelength channels and bends using $\varepsilon$-near-zero materials, Phys. Rev. Lett. 97 (2006) 157403.
10. V.C. Nguyen, L. Chen, K. Halterman, Total transmission and total reflection by zero index metamaterials with defects, Phys. Rev. Lett. 105 (2010) 233908.
11. P. Moitra, Y. Yang, Z. Anderson, I.I. Kravchenko, D.P. Briggs, J. Valentine, Realization of an all-dielectric zero-index optical metamateria, Nature Photonics 7 (2013) 791–795.
12. C. Caloz, T. Itoh, Electromagnetic metamaterials: transmission line theory and microwave applications, Wiley, New York, 2004.
13. T. Hand, S. Cummer, Characterization of tunable metamaterial elements using MEMS switches, IEEE Antennas Wirel. Propag. Lett. 6 (2007) 401–404.
14. J.D. Joannopoulos, S.G. Johnson, J.N. Winn, R.D. Meade, Photonic crystals: molding the flow of light, Princeton University Press, Princeton, 2011.
15. Y. Rahmat-Samii, H. Mosallaei, Electromagnetic band-gap structures: classification, characterization, and applications, Antennas and Propagation, 2001. Eleventh International Conference on (IEE Conf. Publ. No. 480), Manchester, IET 2, 2001, pp. 560–564.
16. B.A. Munk, Frequency selective surface: theory and design, John Wiley and Sons, New York, 2000.
17. F. Yang, Z.L. Mei, T.Y. Jin, T.J. Cui, DC electric invisibility cloak, Phys. Rev. Lett. 109 (2012) 053902.
18. J.M. Lukens, D.E. Leaird, A.M. Weiner, A temporal cloak at telecommunication data rate, Nature 498 (2013) 205–208.
19. R. Schittny, M. Kadic, T. Bückmann, M. Wegener, Invisibility cloaking in a diffusive light scattering medium, Science 345 (2014) 427–429.
20. H. Xu, X. Shi, F. Gao, H. Sun, B. Zhang, Ultrathin three-dimensional thermal cloak, Phys. Rev. Lett. 112 (2014) 054301.
21. M. Gharghi, C. Gladden, T. Zentgraf, Y. Liu, X. Yin, J. Valentine, X. Zhang, A carpet cloak for visible light, Nano Lett. 11 (2011) 2825–2828.
22. X. Chen, H.F. Ma, X.Y. Zou, W.X. Jiang, T.J. Cui, Three-dimensional broadband and highdirectivity lens antenna made of metamaterials, J. Appl. Phys. 110 (2011) 044904.
23. C. García-Meca, A. Martínez, U. Leonhardt, Engineering antenna radiation patterns via quasi-conformal mappings, Opt. Express 19 (2011) 23743–23750.
24. H.F. Ma, X. Chen, X.M. Yang, W.X. Jiang, T.J. Cui, Design of multibeam scanning antennas with high gains and low sidelobes using gradient-index metamaterials, J. Appl. Phys. 107 (2010) 014902.
25. H.F. Ma, T.J. Cui, Three-dimensional broadband and broad-angle transformation-optical lens, Nat. Commun. 1 (2010) 124.
26. F. Yang, Z.L. Mei, T.J. Cui, Design and experiment of perfect relay lens based on the Schwarz-Christoffel mapping, Appl. Phys. Lett. 104 (2014) 073510.
27. C. Lu, Z.L. Mei, Multi-functional lens based on conformal mapping, Opt. Express 23 (2015) 19901–19910.
28. N. Kundtz, D.R. Smith, Extreme-angle broadband metamaterial lens, Nat. Mater. 9 (2010) 129–132.
29. Y. Lai, H.Y. Chen, D.Z. Han, J.J. Xiao, Z.-Q. Zhang, C.T. Chan, Illusion optics: the optical transformation of an object into another object, Phys. Rev. Lett. 102 (2009) 253902.
30. W.X. Jiang, T.J. Cui, Radar illusion via metamaterials, Phys. Rev. E 83 (2011) 026601.
31. Q. Ma, Z.L. Mei, S.K. Zhu, T.Y. Jin, T.J. Cui, Experiments on active cloaking and illusion for laplace equation, Phys. Rev. Lett. 111 (2013) 173901.
32. B.S. Song, S. Noda, T. Asano, Photonic devices based on in-plane hetero photonic crystals, Science 300 (2003) 1537–1537.

33. F. Bonaccorso, Z. Sun, T. Hasan, A.C. Ferrari, Graphene photonics and optoelectronics, Nature Photonics 4 (2010) 611–622.
34. H.T. Chen, W.J. Padilla, J.M. Zide, A.C. Gossard, A.J. Taylor, R.D. Averitt, Active terahertz metamaterial devices, Nature 444 (2006) 597–600.
35. H. Tao, E.A. Kadlec, A.C. Strikwerda, K. Fan, W.J. Padilla, R.D. Averitt, E.A. Shaner, X. Zhang, Microwave and terahertz wave sensing with metamaterials, Opt. Express 19 (2011) 21620–21626.
36. T. Niu, W. Withayachumnankul, A. Upadhyay, P. Gutruf, D. Abbott, M. Bhaskaran, S. Sriram, C. Fumeaux, Terahertz reflectarray as a polarizing beam splitter, Opt. Express 22 (2014) 16148–16160.
37. T. Yang, H. Chen, X. Luo, H. Ma, Superscatterer: enhancement of scattering with complementary media, Opt. Express 16 (2008) 18545–18550.
38. J.B. Pendry, D. Schurig, D.R. Smith, Controlling electromagnetic fields, Science 312 (2006) 1780–1782.
39. W.X. Jiang, C.-W. Qiu, T.C. Han, S. Zhang, T.J. Cui, Creation of ghost illusions using wave dynamics in metamaterials, Adv. Funct. Mater. 23 (2013) 4028–4034.
40. R. Liu, C. Ji, J.J. Mock, J.Y. Chin, T.J. Cui, D.R. Smith, Broadband ground-plane cloak, Science 323 (2009) 366–369.
41. H.F. Ma, T.J. Cui, Three-dimensional broadband ground-plane cloak made of metamaterials, Nat. Commun. 1 (2010) 21.
42. A. Alù, Mantle cloak: invisibility induced by a surface, Phys. Rev. B 80 (2009) 245115.
43. J. Zhang, Z.L. Mei, W.R. Zhang, F. Yang, T.J. Cui, An ultrathin directional carpet cloak based on generalized Snell's law, Appl. Phys. Lett. 103 (2013) 151115.
44. T.J. Cui, M.Q. Qi, X. Wan, J. Zhao, Q. Cheng, Coding metamaterials, digital metamaterials and programmable metamaterials, Light Science & Applications 3 (2014) e218.
45. B.-I. Popa, S.A. Cummer, Cloaking with optimized homogeneous anisotropic layers, Phys. Rev. A 79 (2009) 023806.
46. A. Mirzaei, A.E. Miroshnichenko, I.V. Shadrivov, Y.S. Kivshar, Superscattering of light optimized by a genetic algorithm, Appl. Phys. Lett. 105 (2014) 011109.
47. R.-B. Hwang, H.-T. Huang, Scattering characteristics of cylindrical metamaterials, AIP Advances 6 (2016) 035107.
48. D. Schurig, J.J. Mock, B.J. Justice, S.A. Cummer, J.B. Pendry, A.F. Starr, D.R. Smith, Metamaterial electromagnetic cloak at microwave frequencies, Science 314 (2006) 977–980.
49. C. Li, X.K. Meng, X. Liu, F. Li, G.Y. Fang, H.Y. Chen, C.T. Chan, Experimental realization of a circuitbased broadband illusion-optics analogue, Phys. Rev. Lett. 105 (2010) 233906.
50. W.X. Jiang, H.F. Ma, Q. Cheng, T.J. Cui, Illusion media: generating virtual objects using realizable metamaterials, Appl. Phys. Lett. 96 (2010) 121910.
51. M. Liu, Z.L. Mei, X. Ma, T.J. Cui, DC illusion and its experimental verification, Appl. Phys. Lett. 101 (2012) 051905.
52. G.D. Bai, Z. Zhang, F. Yang, Z.L. Mei, Magnification device for Laplace equation by using homogeneous and isotropic media with positive values, J. Phys. D: Appl. Phys. 48 (2015) 325104.
53. W.X. Jiang, T.J. Cui, X.M. Yang, H.F. Ma, Q. Cheng, Shrinking an arbitrary object as one desires using metamaterials, Appl. Phys. Lett. 98 (2011) 204101.
54. W.X. Jiang, T.J. Cui, Moving targets virtually via composite optical transformation, Opt. Express 18 (2010) 5161–5167.
55. J. Li, J.B. Pendry, Hiding under the carpet: a new strategy for cloaking, Phys. Rev. Lett. 101 (2008) 203901.
56. Y. Luo, J. Zhang, H. Chen, L. Ran, B.I. Wu, J.A. Kong, A rigorous analysis of plane-transformed invisibility cloaks, IEEE Trans. Antennas Propag. 57 (2009) 3926–3933.
57. F. Magnus, B. Wood, J. Moore, K. Morrison, G. Perkins, J. Fyson, M.C.K. Wiltshire, D. Caplin, L.F. Cohen, J.B. Pendry, A dc magnetic metamaterial, Nature Mater. 7 (2008) 295.
58. C. Navau, D.X. Chen, A. Sanchez, N. Del-Valle, Magnetic properties of a dc metamaterial consisting of parallel square superconducting thin plates, Appl. Phys. Lett. 94 (2009) 242501.
59. F. Gömöry, M. Solovyov, J. Šouc, C. Navau, J. Prat- Camps, A. Sanchez, Experimental realization of a magnetic cloak, Science 335 (2012) 1466.
60. S. Narayana, Y. Sato, DC magnetic cloak, Adv. Mater. 24 (2012) 71.
61. L. Zeng, Y. Zhao, Z. Zhao, H. Li, Electret electrostatic cloak, Physica B: Condens. Matter 462 (2015) 70–75.
62. C. Lan, Y. Yang, Z. Geng, B. Li, J. Zhou, Electrostatic field invisibility cloak, Sci. Rep. 5 (2015).
63. T.C. Han, X. Bai, D.L. Gao, J.T.L. Thong, B.W. Li, C.-W. Qiu, Experimental demonstration of a bilayer thermal cloak, Phys. Rev. Lett. 112 (2014) 054302.
64. T.C. Han, X. Bai, J.T.L. Thong, B. Li, C.-W. Qiu, Full control and manipulation of heat signatures: cloaking, camouflage and thermal metamaterials, Adv. Mater. 26 (2014) 1731.
65. T.H. Chen, F. Yang, Z.L. Mei, A simple and flexible thermal illusion device and its experimental verification, Phys. Status Solidi A 212 (2015) 1746–1750.
66. F. Sun, S. He, Transformation magneto-statics and illusions for magnets, Sci. Rep. 4 (2014).
67. S. Zhang, C. Xia, N. Fang, Broadband acoustic cloak for ultrasound waves, Phys. Rev. Lett. 106 (2011) 024301.
68. S.A. Cummer, B.I. Popa, D. Schurig, D.R. Smith, J.B. Pendry, M. Rahm, A. Starr, Scattering theory derivation of a 3D acoustic cloaking shell, Phys. Rev. Lett. 100 (2008) 024301.
69. H. Chen, C.T. Chan, Acoustic cloaking in three dimensions using acoustic metamaterials, Appl. Phys. Lett. 91 (2007) 183518.
70. N.F. Yu, G. Patrice, M.A. Kats, F. Aieta, J.P. Tetienne, F. Capasso, Z. Gaburro, Light propagation with phase discontinuities: generalized laws of reflection and refraction, Science 334 (2011) 333–337.
71. Y. Zhao, A. Alù, Manipulating light polarization with ultrathin plasmonic metasurfaces, Phys. Rev. B 84 (2011) 205428.
72. P.Y. Chen, A. Alù, Mantle cloaking using thin patterned metasurfaces, Phys. Rev. B 84 (2011) 205110.
73. A.V. Kildishev, A. Boltasseva, V.M. Shalaev, Planar photonics with metasurfaces, Science 339 (2013) 1232009.
74. N. Yu, F. Capasso, Flat optics with designer metasurfaces, Nat. Mater. 13 (2014) 139–150.
75. D. Lin, P. Fan, E. Hasman, M.L. Brongersma, Dielectric gradient metasurface optical elements, Science 345 (2014) 298–302.
76. G. Mie, Pioneering mathematical description of scattering by spheres, Ann. Phys. 25 (1908) 337.
77. Y.R. Padooru, A.B. Yakovlev, P.Y. Chen, A. Alù, Analytical modeling of conformal mantle cloaks for cylindrical objects using sub-wavelength printed and slotted arrays, J. Appl. Phys. 112 (2012) 034907.

78. B. Zhang, Y. Luo, X. Liu, G. Barbastathis, Macroscopic invisibility cloak for visible light, Phys. Rev. Lett. 106 (2011) 033901.
79. N.M. Estakhri, A. Alù, Ultra-thin unidirectional carpet cloak and wavefront reconstruction with graded metasurfaces, IEEE Antennas Wirel. Propag. Lett. 13 (2014) 1775–1778.
80. L.Y. Hsu, T. Lepetit, B. Kanté, Extremely thin dielectric metasurface for carpet cloaking, Progress Electromagn. Res. 152 (2015).
81. X. Ni, Z.J. Wong, M. Mrejen, Y. Wang, X. Zhang, An ultrathin invisibility skin cloak for visible light, Science 349 (2015) 1310–1314.
82. D.S. Weile, E. Michielssen, Genetic algorithm optimization applied to electromagnetics: A review, IEEE Trans. Antennas Propag. 45 (1997) 343–353.
83. X. Wang, F. Chen, E. Semouchknika, Spherical cloaking using multilayer shells of ordinary dielectrics, AIP Advances 3 (2013) 112111.
84. X. Wang, E. Semouchkina, A route for efficient non-resonance cloaking by using multilayer dielectric coating, Appl. Phys. Lett. 102 (2013) 113506.
85. Z. Yu, Y. Feng, X. Xu, J. Zhao, T. Jiang, Optimized cylindrical invisibility cloak with minimum layers of non-magnetic isotropic materials, J. Phys. D: Appl. Phys. 44 (2011) 185102.
86. S. Xu, X. Cheng, S. Xi, R. Zhang, H.O. Moser, Z. Shen, Y. Xu, Z. Huang, X. Zhang, F. Yu, B. Zhang, H. Chen, Experimental demonstration of a free space cylindrical cloak without superluminal propagation, Phys. Rev. Lett. 109 (2012) 223903.
87. S. Liu, H.X. Xu, H.C. Zhang, T.J. Cui, Tunable ultrathin mantle cloak via varactor-diode-loaded metasurface, Opt. Express 22 (2014) 13403.
88. F.G. Vasquez, G.W. Milton, D. Onofrei, Broadband exterior cloaking, Opt. Express 17 (2009) 14800.
89. M. Selvanayagam, G.V. Eleftheriades, Experimental demonstration of active electromagnetic cloaking, Phys. Rev. X 3 (2013) 041011.
90. J.C. Howell, J.B. Howell, J.S. Choi, Amplitude-only, passive, broadband, optical spatial cloaking of very large objects, Appl. Opt. 53 (2014) 1958.
91. J.S. Choi, J.C. Howell, Paraxial ray optics cloaking, Opt. Express 22 (2014) 29465.
92. T. Tyc, S. Oxburgh, E.N. Cowie, G.J. Chaplain, G. Macauley, C.D. White, J. Courtial, Omnidirectional transformation-optics cloak made from lenses and glenses, JOSA A 33 (2016) 1032.

**Cite this article as**: Lu C, Mei ZL, Tang WX & Cui TJ: Manipulating scattering features by metamaterials. EPJ Appl. Metamat. 2016, **3**, 3.